https://doi.org/10.15407/ufm.23.04.684

I.E. VOLOKITINA [1,*], A.V. VOLOKITIN [2,], and E.A. PANIN [2,***]**
[1] Rudny Industrial Institute,
50 Let Oktyabrya Str., 38; 111500 Rudny, Kazakhstan
[2] Karaganda Industrial University,
Republic Ave., 30; 101400 Temirtau, Kazakhstan
* i.volokitina@alservice.kz, ** a.volokitin@tttu.edu.kz, *** ye.panin@tttu.edu.kz

MARTENSITIC TRANSFORMATIONS IN STAINLESS STEELS

Currently, the direction of materials' research, in which the martensitic transformations are observed, is intensively developed. This is due to the fact that, in the martensitic-transformation process, various defects of crystal structure (twins, dislocations, packaging defects, *etc.*) are formed in many materials, which together with grain fragmentation lead to a significant increase in the strength properties. The widespread occurrence of martensitic transformations has led to the study of the defective microstructure features and changes in the mechanical properties in the martensitic transformation process. This allowed the theory of martensitic transformations to occupy a key place in the science of the structure and properties of crystalline bodies. The operating temperature range of steels of this class is limited from below by their tendency to low-temperature embrittlement (cold breaking) under radiation effects, and from above, by the level of long-term strength (heat resistance). In this regard, today, the increased attention of specialists in the field of condensed matter physics to ferritic–martensitic steels is caused by the need to identify the mechanisms for the formation of microstructures and functional properties of steels stable at operating temperatures, as well as to search for reserves to increase their heat resistance, while maintaining a sufficient plasticity level.

Keywords: stainless steel, martensite, martensitic transformation, microstructure, annealing, heat resistance.

1. Introduction

Martensitic transformations are the most widely for the Fe-based alloys. Martensitic transformation in steel is a polymorphic transformation that is observed during rapid cooling from the high–temperature γ-phase (austenite) to the low-temperature α-phase (martensite). Martensite is the main structural component of hardened steel.

Citation: I.E. Volokitina, A.V. Volokitin, and E.A. Panin, Martensitic Transformations in Stainless Steels, *Progress in Physics of Metals*, **23**, No. 4: 684–728 (2022)

Martensitic transformation occurs at certain temperatures. These temperatures are different for different materials. During cooling, the M_s point is the start temperature of the martensitic transformation, and the M_f point is the finish temperature of the martensitic transformation. The position of the M_s point does not depend on the cooling rate. At temperature M_s, the transformation is just beginning, and the first martensite crystals appear. In order for the martensitic transformation to be developed, it is necessary to continuously cool carbon steel in the temperature range M_s–M_f. If cooling is suspended and carbon steel is maintained at a constant temperature within this interval, the formation of martensite stops almost immediately. To resume the transformation, it is necessary to lower the temperature further in the martensitic interval M_s–M_f [1].

Some alloying elements can both reduce and increase the point of martensitic transformation. Therefore, for example, in alloy steels containing a sufficient amount of carbon and alloying elements, the M_s point is located below 0 °C; using the quenching, it is possible to obtain a completely austenitic structure. Thus, the required temperature for the formation of martensite depends on the chemical composition of steel.

The martensitic transformation during cooling does not go through to the end; a certain volume fraction of austenite remains in the steel, which eventually does not turn into martensite. This austenite is called residual austenite, and its amount increases with a decrease in the M_s point.

Stainless (corrosion-resistant) and heat-resistant steels and alloys based on iron and nickel are the most important category of special structural materials that have found application in many industries. Increased resistance against uniform corrosion in a wide range of corrosive media of varying degrees of aggressiveness is a distinctive feature of stainless and heat-resistant steels and alloys.

The main alloying element that gives steel corrosion resistance in oxidizing environments is chromium. Chromium contributes to the formation of a protective dense passive film of Cr_2O_3 oxide on the surface of stainless steel. A film thickness sufficient to give corrosion resistance to stainless steel is formed when at least 12.5% chromium is added to the alloy.

The cost of chromium is relatively low; it is not a scarce component. Therefore, chromium-plated stainless steels are relatively inexpensive and find the widest application in industry, having a fairly good set of technological properties. Elements of equipment operating at high pressure and temperature under the influence of aggressive environments are made of chrome-plated stainless steels.

As known, plastic deformation is a complex physical-chemical process, because of which along with a change in the shape and structure of the initial state, its physical-chemical and mechanical properties change.

Under the most diverse types and modes of plastic deformation in crystalline materials with different types of crystal lattice, a fundamental phenomenon of fragmentation is observed, *i.e.*, deformation grinding of the structure of materials of the order up to 100–200 nm [2–8]. The phenomenon of deformation grinding (fragmentation) is based on modern hardening processing technologies, such as rolling, drawing, *etc.* This leads not only to a sharp increase in strength, but also to an increase in plasticity. Modern methods of pressure treatment of steels with a b.c.c. lattice are studied in detail in Refs. [9–11]. According to the authors of these works, ultrafine-grained (UFG) steels with a grain size of less than 1 micron have high strength and significant impact strength compared to traditional composite steels, and therefore these materials are currently the subject of extensive research worldwide. UFG steel can be produced as a result of thermomechanical processes or by the method of severe plastic deformation. The paper [12] describes various advanced methods for producing ultrafine-grained b.c.c. steels. Nevertheless, the issue of obtaining submicro- and nanocrystalline materials with specified microstructure parameters and mechanical properties remains very relevant, and this is primarily due to the insufficient development of the physics of severe plastic deformation, in which the processes of grinding the initial structure of materials to the nanoscale occur.

Long-term studies of the fragmentation phenomenon have allowed concluding that its root cause is powerful elastic stresses in polycrystals, the sources of which arise at the grain boundaries and joints. In essence, fragmentation is the result of plastic accommodation, the heterogeneity of which in the grain volume manifests itself in the fragmented substructure form. The emergence of new boundaries near the joints or morphological features of the initial boundaries (steps, ledges, bends) is observed, which germinate inside the grains and divide them into disoriented crystal elements. The sources of internal stresses (plastic incompatibilities) accumulate at the boundaries due to differences in the intrinsic plastic deformations of adjacent grains. The appearance of such incompatibilities is inevitable, because crystal grains are oriented differently with respect to macroscopic deforming stresses and therefore exhibit different plastic malleability. However, as the disorientation between the fragments that have arisen grows, the process described above is reproduced already at their borders and joints, forming a new generation of fragments, *etc.* An important role in the fragmentation process of the crystal lattice during the formation of a submicrocrystalline structure is played by the dislocation-disclosure mechanism of reorientation of the crystal lattice, including the formation of the above substructures with a high excess density of dislocations of one sign and their subsequent rearrangements into localized boundaries of disorientation [13].

Thus, a fragmented substructure is a substructure of mutually disoriented regions (subgrains) separated by small-angle and medium-angle dislocation subboundaries (fragment walls). Fragmented substructure is formed both because of heat treatment and during steel deformation [14].

2. Current Concepts on Martensitic Transformation

Martensitic transformation is one of the main methods of metal hardening; therefore, considerable attention has been paid to the study of the features of its course. Especially, the works of G.V. Kurdyumov school can be highlighted, according to which, the theory of martensitic transformations was laid in the forties of the last century, based on the generalization of numerous experiments results. It was also found that martensitic transformation can occur not only during cooling, but also during plastic deformation, which leads to the emergence of a number of new phenomena, which include the following [15]:

• expansion of the temperature range, *i.e.*, the appearance of such phases that are not observed at a given temperature;

• changing the kinetics of martensitic transformations;

• the emergence of new phases (*e.g.*, ε-martensite, the features of the appearance of which will be discussed later);

• change of mechanical properties (superplasticity, shape memory effect).

The main component of structural high-strength low-carbon steels is martensite. The transformation of austenite into martensite is realized in the case of significant supercooling below the critical point A_1 and during the cooling at a rate that suppresses the decay of austenite by pearlite and intermediate mechanisms. By its mechanism, the martensitic transformation is a diffusionless-shift phase transformation characterized by an ordered, interconnected nature of the atoms movement at distances less than interatomic without the exchange of atoms in places [16] (in contrast to the atomic-diffusion-caused processes in metals and alloys, see, *e.g.*, Refs. [17–28]).

Despite the fact that the martensitic transformation reflects the general laws of phase transformations, it has a number of features due to the desire of the system to minimize free energy:

• there is a certain orientation relationship between the lattices of martensite (M) and austenite (A): $(111)_A \parallel (110)_M$ and $[110]_A \parallel [111]_M$ (Kurdyumov–Sachs ratio);

• the most typical, equilibrium form of martensitic crystals is a plate with a small ratio of thickness to other sizes;

• the habitus plane of the martensite plate has a certain orientation relative to the crystal lattice of the initial phase;

• a characteristic relief is formed on the flat polished surface of the sample during martensitic transformation, which is due to a change in the shape of the transformed volume;

• domenization of a martensitic crystal with the formation of twin orientations with different intrinsic deformations and low energy boundaries, *i.e.*, the formation of a regular crystal substructure;

• martensitic crystals are prone to an ordered mutual arrangement, *i.e.*, to the formation of ensembles.

Depending on the steels chemical composition, it is possible to form martensite of various morphologies, determined by a combination of shape, fine structure and the articulation method into crystal ensembles [29].

When studying the structure of hardened carbon steels, two main morphological martensite types are distinguished, namely, rack-and-pinion (also called batch, massive, dislocation) and plate (needle, twinned, low-temperature) ones.

Rack-and-pinion martensite, which has the greatest applied value, is formed during the hardening of structural low- and medium-carbon steels, iron and its moderate and high-alloy alloys, *i.e.*, in steels with a high martensitic point (M_s above 100 °C), as well as in martensitic-ageing steels. At the same time, parallel rails resulting from a homogeneous shift are stretched in the direction $\langle 111\rangle\alpha \parallel \langle 011\rangle\gamma$ and form a package whose linear dimensions depend on the size of the austenitic grain, but they differ little in different directions and are most often within 3–20 microns.

The thickness of the plates (rails) in carbon and nickel steels is in the range from 0.1 to 2.25 microns, more often it is 0.1–0.2 microns [41]. The traditional dimensions ratio of the rail is 1÷7÷30, *i.e.*, the length of the rail is of 4–5 times of its width [31]. The density of crystal structure defects (dislocations) inside the plate of batch martensite is very high (about 10^{11}–10^{12} cm^{-2}), which is why batch martensite is sometimes called dislocation.

The structure of the martensite package is such that the adjacent rails are oriented almost identically (the misorientation angle is up to 2–3°) and are separated along the plane $\{110\}\alpha \parallel \{111\}\gamma$ by small-angle dislocation boundaries (mainly torsion boundaries) [32]. At the same time, the ratio of the number of high-angle to low-angle boundaries in a 0.2% C steel martensite package is 1–5, *i.e.* 5/6 of all interstitial boundaries are permeable to dislocations [33]. The packages are separated by a relatively homogeneous irregular boundary with inclusions of sites of good coupling; the proportion of small-angle disorientations is 6%, 17% of disorientations close to regular ones. Thus, it can be concluded that the share of high-angle boundaries between packages is 77%.

As shown in Refs. [34, 35], the method of grouping crystals into a

package is determined from the minimum energy condition; the package is not a complex of arbitrarily oriented martensitic rails, but a conglomerate of self-consistent crystals, the formation of which minimizes both dilation associated with Bain deformation and shear stresses arising during martensitic transformation. Due to this, the stresses fields are largely compensated within each package and do not affect the boundaries of the former austenitic grains.

3. Martensite Heat Treatment Features

The standard heat treatment for ferritic–martensitic steels is quenching (normalization) and subsequent high-temperature tempering [36]. Normalization consists in austenization at a temperature above the critical point A_{c1} (start temperature of the ferrite transformation (b.c.c. structure) into austenite (f.c.c. structure)) and air-cooling. For steels with Cr content of 5–12%, such treatment leads to the martensite formation ('SCT' structure) with a high dislocation density [37, 38]. The tempering temperature for steel is chosen in such a way as to dissolve the carbides of $Me_{23}C_6$, but avoid the δ-ferrite formation. Figure 1 shows a typical microstructure of EK-181 steel with 12% Cr content after quenching from a temperature of 1100 °C and tempering at 500 °C. It was shown in Ref. [39] that, after quenching from a temperature of 980 °C and 1180 °C, a completely martensitic structure is formed in 9% Cr steels, whereas an increase in the quenching temperature to 1280 °C leads to the appearance of up to 20% δ-ferrite in the structure (Fig. 2). The formation of batch martensite occurs within the boundaries of former austenitic grains with a size of 25–40 microns [39, 40].

Tempering at a temperature of 650–780 °C for 1–3 hours leads to the formation of a ferritic–martensitic structure. Carbides $M_{23}C_6$ (where M is Cr, Fe, Mn), 60–200 nm in size, and smaller carbonitrides MX (M is V, X is C or N), 20–80 nm in size, are isolated. There is a partial return of the dislocation structure, the average width of the martensite plates increases.

In work [38], the authors associate an increase in the strength and thermal stability of EK-181 steel with a high density of nanoscale particles of vanadium carbonitride V(CN), the release of which occurs after tempering at 720 °C. In steels containing W and Mo, the Laves phases may be present as Fe_2M intermetallic compounds (Fe_2W and Fe_2Mo). Their secretions are detected during prolonged high-temperature annealing, as well as creep tests [42]. After the tempering, Laves phases are not detected.

The phase transformation ($\gamma\rightarrow\alpha'$) of EK-181 steel occurs in the temperature range of 300–400 °C. The presence of ferrite-forming elements Cr, V and Ta in steel shifts the critical points A_{c1} and A_{c3} ($\alpha\rightarrow\gamma$) by sev-

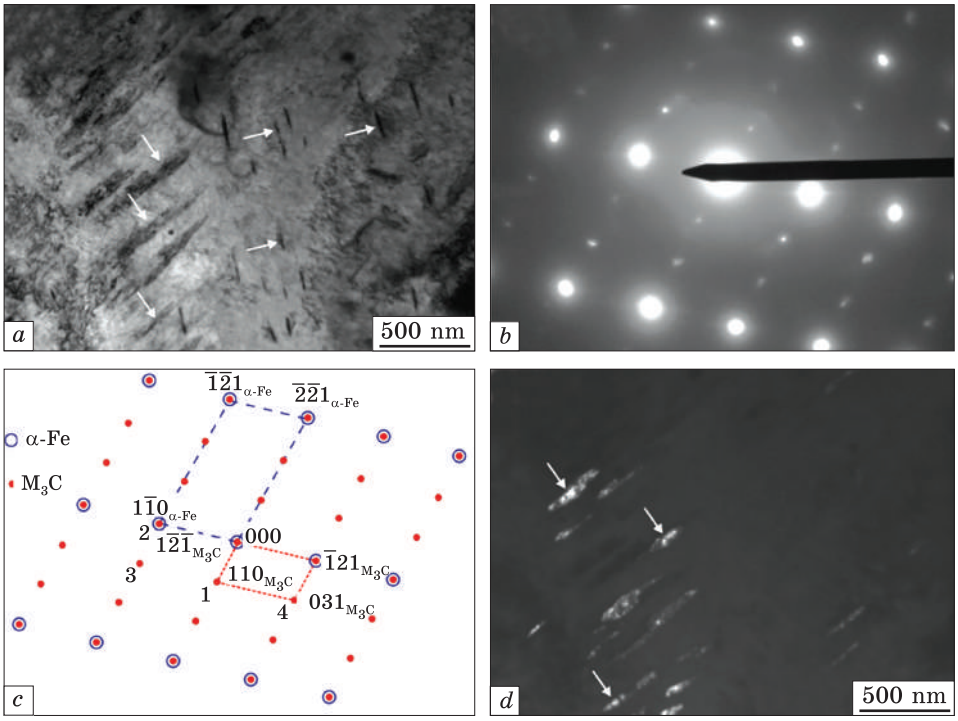

Fig. 1. Microstructure of EK-181 steel after quenching in air from 1100 °C and tempering at 500 °C for 1 hour: light-field image (*a*); and corresponding microdiffraction pattern and its decoding (*b, c*); dark-field image in the reflex (*1*) of carbide M_3C [41]

eral hundred degrees [43], compared with unalloyed high chromium 12% Cr steels. Austenization under heating ends at a temperature of 910 °C. Exposure at a temperature of 1050–1100 °C leads to the dissolution of carbides. According to Fig. 1, non-metallic phases $M_{23}C_6$, V(CN), and M_3C are present in the microstructure of EK-181 steel after quenching and tempering. After quenching from 1100 °C, the main structural components of steel are ferrite and martensite.

In work [44], the features of the carbide subsystem after various heat treatment modes, the influence of various heat treatment modes on the microstructure and mechanical properties of EK-181 steel were studied. The authors found that an increase in the quenching rate in combination with subsequent step annealing at low temperatures leads to quantitative changes in the structure. The study of several heat treatment modes showed that the highest values of short-term strength are shown by samples hardened in water and then tempered in a step mode (500 °C, 1 hour + 600 °C, 1 hour + 720 °C, 1 hour). The authors explain this by the fact that, under such conditions, the separation of nanoscale

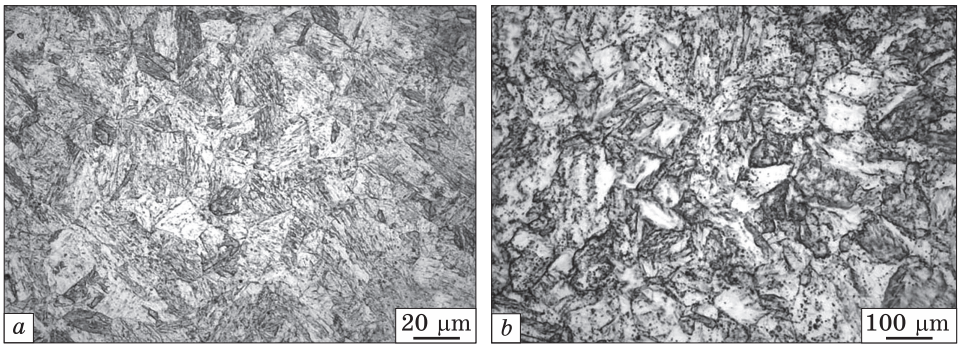

Fig. 2. Microstructure of steel 9Cr–0.09C–0.56Mn–0.23V–1W–0.063Ta–0.02N (wt.%): optical micrograph of a sample normalized at 1253 K/2 h, martensitic structure (*a*) and optical micrograph of a sample normalized at 1253 K/2 h followed by tempering at 1033 K for 30 min (*b*) [39]

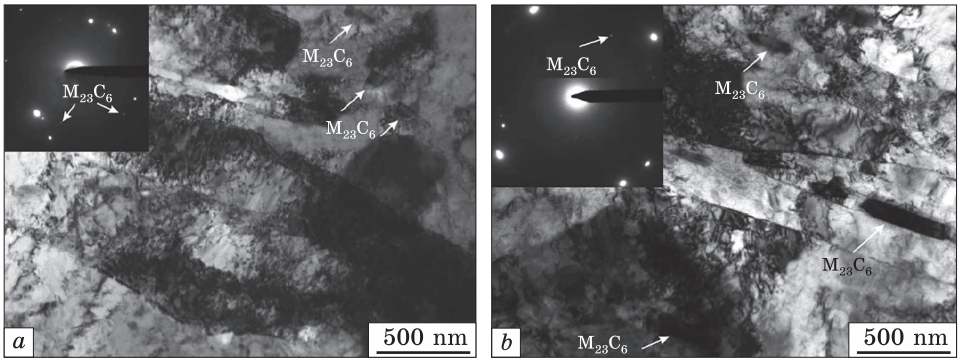

Fig. 3. Microstructure of EK-181 steel after step-by-step treatments, light-field images and corresponding microdiffraction patterns: 1100 °C quenching in water, tempering (500 °C, 1 hour + 600 °C, 1 hour + 720 °C, 1 hour) (*a*) and 1100 °C quenching in water, tempering (620 °C, 1 hour + 720 °C, 1 hour) (*b*) [44]

particles V(CN) occurs under thermodynamically more nonequilibrium conditions, which leads to an increase in density and an increase in the dispersion of the heterophase structure. At the same time, reducing the annealing time during step annealing allows reducing the intensity of martensite tempering. According to electron-microscopy studies (Fig. 3), such a reduction leads to a significant decrease in the volume fraction of ferrite, a decrease in the transverse dimensions of the martensite lamellae. There is also an increase in the dislocation density, but at the same time, the dispersion of $M_{23}C_6$ carbides decreases, and the particle density V(CN) increases, compared with standard heat treatment modes. Such microstructural features lead to an increase in the yield strength by more than 20% (750 MPa and 820 MPa), including high-temperature yield strength (425 MPa at 650 °C).

Authors of work [45] investigated the effect of alloying elements on the heat-resistant properties of martensitic steels with a chromium content of 9–12%, which have a high creep resistance, a low coefficient of thermal expansion at a relatively low cost, which makes their use in thermal energy very attractive [46].

One of the ways to increase operating temperatures is the introduction of dispersed nanoparticles resistant to coagulation, which leads to the occurrence of threshold stresses below which deformation does not occur. This mechanism is explained by the dislocations inability to bypass quickly particles with a size of 10–40 nm due to crawling. To overcome the dislocation particles, they are forced to generate loops, which require additional stresses. Threshold stresses are inversely proportional to the distance between the particles. The increase in threshold stresses is proportional to the volume of dispersed particles of the second phases and their grinding. Thus, a solid solution with dispersed particles that reduce the diffusion rate, an increase in the specific volume and size of nanoparticles are necessary conditions for increasing the creep limit of heat-resistant materials [45].

Another important creep characteristic is the time to failure. The greatest influence on it is exerted by the processes of grain boundary sliding (GBS), which leads to the pores formation of deformation origin along the grain boundaries [47, 48]. An increase in this characteristic is achieved when the conditions are met:

• the suppression of GBS processes due to microalloying of steels with boron or the separation of dispersed particles with a size of 10 nm;

• achieving the optimal grain size, which will prevent diffusion creep and the pores formation at the grain boundaries;

• an absence of large solid particles along the grain boundaries.

In addition to the EK-181 steel described above, currently, there are industrial ferritic–martensitic steels, *e.g.*, 12% Cr ferritic–martensitic steels ChS-139 and EI961-Sh as well as their analogues EUVROFER-97 (Fe–8.5Cr–1.0W–0.05Mn–0.25V–0.08Ta–0.05N–0.005B–0.10C), F82H (Fe–7.5Cr–2.0W–0.2V–0.04Ta–0.10C), and ORNL 9Cr–2WVTa (Fe–9Cr–2W–0.25V–0.07Ta–0.10C) [38].

Due to the long-term operation of ferritic–martensitic steels at elevated temperatures, it is necessary to study the thermal stability of their microstructure and physicomechanical properties. Such studies are presented in Ref. [49]. The authors studied the effect of prolonged ageing (13,500 h) at temperatures of 450 and 620 °C of EK-181 and ChS-139 steels after traditional heat treatment (THT) and combined heat treatment (CHT). CHT consists in normalization at 1100 °C (1 hour) and thermal cycling near the critical temperature of the beginning ($\alpha \rightarrow \gamma$) of the transformation of A_{c1}, and further release at 720 °C (1 hour). At the same time, prolonged ageing after THT did not lead to significant

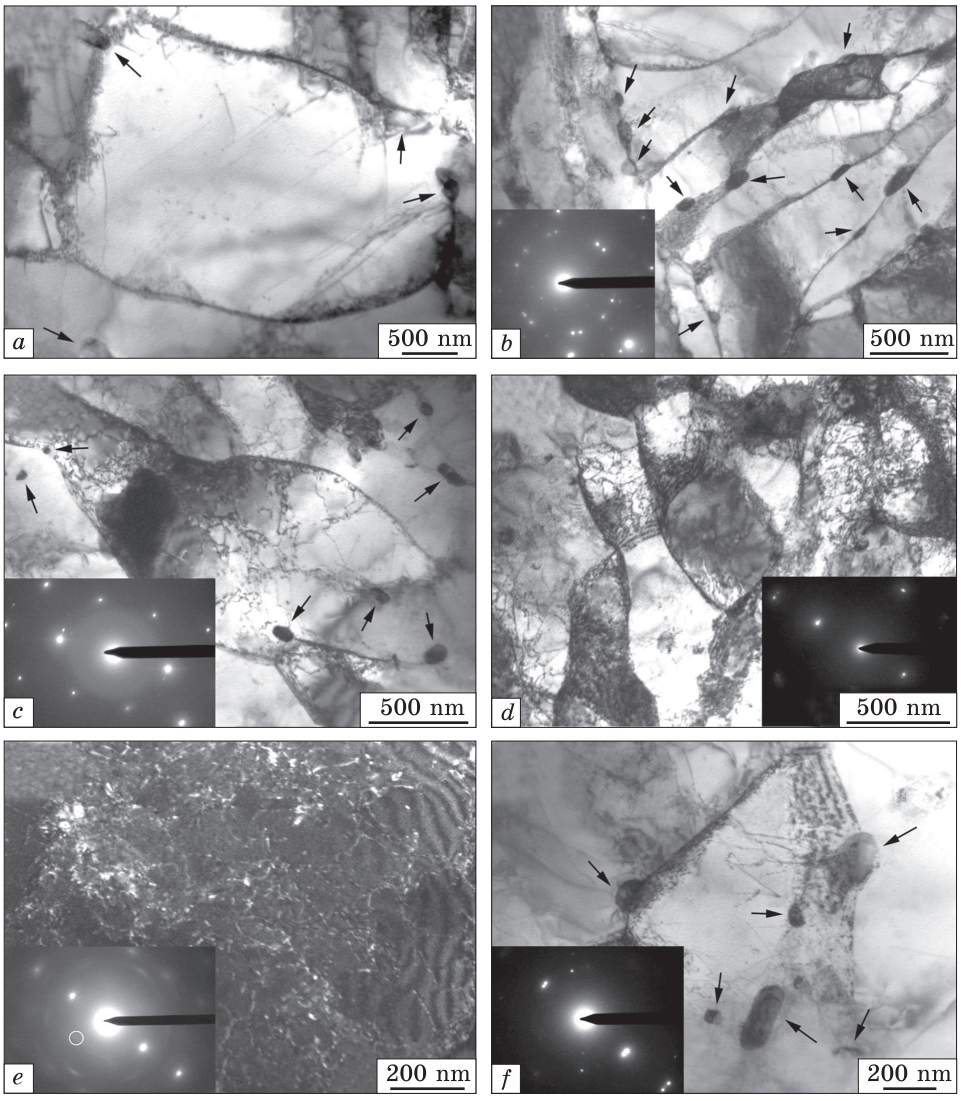

Fig. 4. Microstructure of (*a–c*) EK-181 and (*d–f*) ChS-139 steels after CHT with subsequent ageing at (*a, b, d*) 450 and (*c, e, f*) 620 °C for 13 500 h. Arrows show $M_{23}C_6$ precipitates [49]

microstructural changes. A high density of dislocations has been preserved, the fixation of which occurred on V(CN) particles. After CHT and ageing at 450 °C, the changes are more significant. The beginning recrystallization processes led to an increase in the volume fraction of ferritic grains, the volume fraction of V(CN) particles decreased. The processes of martensite tempering occurred more intensively, the edges of the rails curved and acquired a rounded shape (Fig. 4). The nature of

the distribution of $M_{23}C_6$ carbides, as well as their size and volume fraction did not undergo significant changes. With an increase in the ageing temperature to 620 °C, more intensive nucleation and growth of recrystallized ferrite grains occurred, their size increased 2–3 times compared to ageing at 450 °C. The volume fraction and size of $M_{23}C_6$ carbides have not changed significantly, but they have acquired a more equiaxed shape. The distinctive features of the EK-181 and ChS-139 steels after prolonged ageing were the higher density and dimensions of $M_{23}C_6$ carbides in ChS-139 steel. The yield strength and plasticity after both temperatures of prolonged ageing were comparable with the initial values, which the authors explain by the high density of nanoscale carbonitride particles V(CN).

There is also work [50] comparing the transformations occurring during heating of austenitic steel at different deformation temperatures. Deformation was carried out at ambient and cryogenic temperatures. The results of the study showed that in the high-pressure torsion process at cryogenic and ambient temperatures during the first cycles of deformation, the difference in grain size and structure is not large, since the adiabatic effects are comparable. Only after 4 deformation cycles, when the density of defects increases greatly, cryogenic cooling becomes effective. The structure of samples deformed at both temperatures is grinded to nanostructured, so the deformation of AISI-316 steel at ambient temperature with an average grain size of 32 μm leads to the formation of an equiaxed homogeneous microstructure of 0.5 μm in size, consisting of a mixture of austenite and α-martensite. Deformation at cryogenic temperature leads to the formation of an equiaxial homogeneous microstructure of 0.2 μm in size, consisting of 90% α-martensite with a predominance of large-angle boundaries.

Austenitic steel after annealing at 600 °C demonstrates the optimal combination of ductility and strength, which is necessary for piston rings. Therefore, the following thermomechanical treatment is proposed for the manufacture of piston rings: quenching at 1050 °C, holding for 30 minutes and cooling in water, then, 8 deformation cycles by the high-pressure torsion (HPT) method at cryogenic temperature and annealing at 600 °C. As a result of such processing, the microstructure consists of fine ferrite grains with a size of 0.3 μm and uniformly distributed carbide particles [50].

In work [51], the influence of various microstructural states on the mechanical properties of 9% Cr steel (9Cr–1W–0.06Ta–0.22V–0.08C) was evaluated. The effect of isothermal exposure in the temperature range 973–1473 K was studied, followed by quenching in oil and tempering at 1033 K for 1 hour. It is shown that the smallest size of the austenitic steel grain is formed after exposure in the intercritical temperature range between A_{c1} and A_{c3}, while the plasticity was maximal.

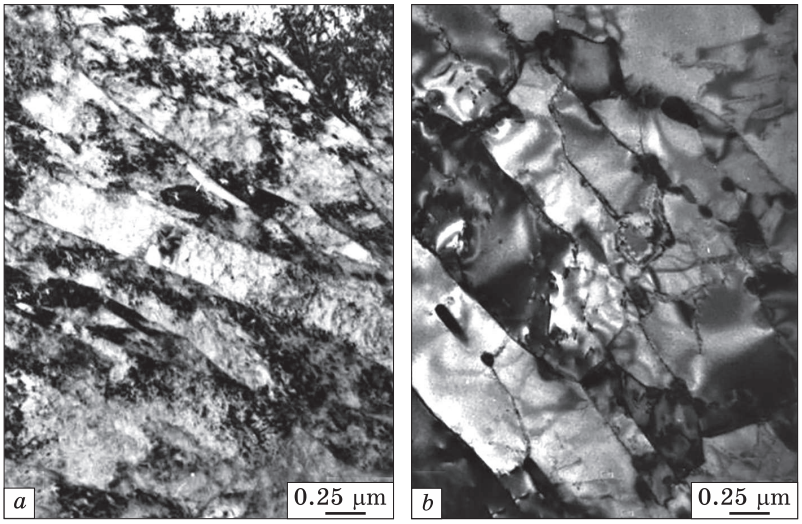

Fig. 5. Defective structure of ferritic–martensitic steel 12Cr–1MoVW (Sandvik HT9) in normalized (*a*) and tempered (*b*) states [52]

With an increase in the heat treatment temperature above A_{c3}, the average grain sizes of the former austenite increase, the hardness and tensile strength of the steel increase, but as a result, the tensile plasticity decreases. These processes are associated with the rapid dissolution of $M_{23}C_6$ carbides at these temperatures.

When developing 9 and 12% chromium steels, it is necessary to maintain a balance between austenitic and ferrite stabilizing elements in order to obtain a 100% austenitic structure during austenization and a 100% martensitic structure after quenching (normalization). Although in some cases, in addition to martensite, a certain amount of δ-ferrite may be present in the steel structure, especially in 12% Cr steels. Chromium is a ferrite stabilizer; therefore, with an increase in its content from 9 to 12%, it is necessary to add austenite stabilizer elements. Carbon is the most popular gamma stabilizer. However, for a new generation of steels, the carbon content is limited to ≈0.15% for better weldability. Therefore, in order to avoid the formation of δ-ferrite, it is necessary to add other γ-stabilizing elements to the steel [52].

The austenization temperature for steels of this class should be, on the one hand, high enough to completely dissolve $M_{23}C_6$ carbides, on the other hand, low enough to avoid the formation of δ-ferrite (high-temperature modification of the b.c.c. phase), which is inherited during cooling. As shown in Ref. [33], normalization of 9% chromium steels at 980 °C and 1180 °C leads to the formation of 100% martensite, while steels hardened from 1280 °C contain ≈20% δ-ferrite. The typical sizes of the former austenitic grains vary in the range from ≈25 to 40 microns [33].

Figure 5 shows electron-microscope images of 12% chromium ferritic–martensitic Sandvik HT9 steel in a normalized and tempered state [52]. After normalization, a typical structure of batch martensite with dimensions (width) of submicron-scale martensitic lamellae and with a high density of dislocations is observed.

To increase the impact strength and ductility, normalized steel is subjected to tempering at a temperature below the critical point Ac_1. For most steels, tempering is carried out at 720–760 °C. During such tempering, $M_{23}C_6$ carbides (M is Cr, Fe, Mo, Mn) and MX carbonitrides (M is V, Nb, Ti, Zr, while X is C, N) are isolated in the ferritic–martensitic matrix (Fig. 5, *b*). $M_{23}C_6$ carbides have dimensions of 60–200 nm and are located mainly along the boundaries of martensitic rails and former austenitic grains. MX particle sizes are 20–80 nm. High-chromium steels may also contain particles of the Laves phase, namely, intermetallides of the Fe_2M type (*e.g.*, Fe_2W and Fe_2Mo in steels containing W and Mo, respectively). However, no such particles were detected after the tempering. According to Ref. [36], they are isolated during long-term high-temperature annealing and creep tests, as a rule, along the boundaries of grains and subgrains. Tempering of steels also leads to a partial return of the dislocation structure; the average width of the martensite rails increases from 0.15–0.2 microns to 0.25–0.5 microns (Fig. 5, *b*). Nevertheless, a sufficiently high dislocation density remains (10^9–10^{11} cm^{-2}, depending on the release conditions) [52]. The control of grain and subgrain sizes, dislocation density, type, density, size and spatial distribution features of carbide phases allows changing the strength and plastic properties of steels in a fairly wide range.

According to Ref. [53], hot deformation of metastable austenite in high-strength steels leads to significant hardening of martensite. This effect is called ausforming. For example, a study of 13% Cr, 0.3% C steel showed that processing, including ausforming, changes the stages of martensite tempering and promotes the release of fine carbides. In this regard, in recent years, a number of papers [54–59] have proposed the use of thermomechanical treatment applied to 9–12% Cr ferritic–martensitic steels to increase their high-temperature strength.

S. Hollner and co-authors are also considering the possibility of modifying the microstructure of ferritic–martensitic steels using thermomechanical treatments on the example of modified steel 9Cr–1Mo (Grade 91) and steel 9Cr–3W–3Co–V–Nb–B–N (NPM) [51, 53]. Traditional heat treatment of Grade 91 steel includes quenching from 1050 °C (30 min exposure) and tempering at 780 °C (1 h exposure); in regard to NPM steel, treatment includes quenching from 1150 °C (1 h exposure) and tempering at 770 °C (4 h exposure). The thermomechanical treatment proposed in Refs. [57, 59] is aimed at grinding austenite grains and enhancing the effect of fixing dislocations by particles of carboni-

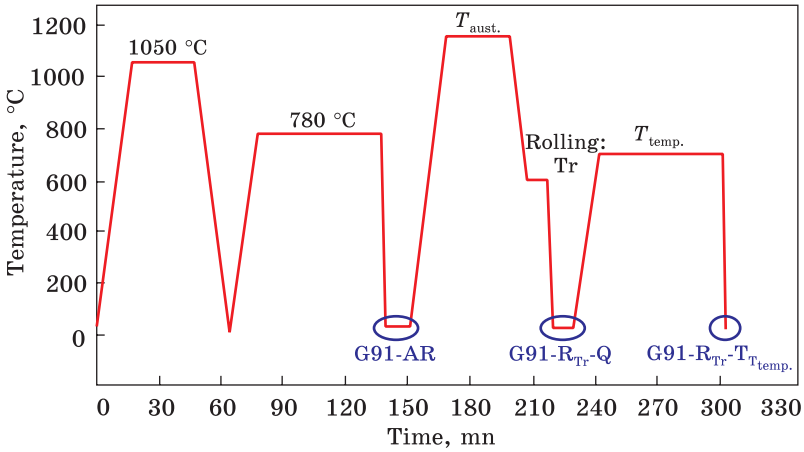

Fig. 6. Diagram of the traditional thermal and subsequent thermomechanical treatment of Grade 91 steel: AR — as-received (traditional treatment); R — rolled state; Q — quenched state; T — tempered state [57]

trides of the *MX* type, for which the deformation of steel in the austenitic region is proposed. Warm rolling is used to increase the dislocations density, grain boundaries and subgrains as places of origin of stable fine particles of the *MX* phase. The schematic diagram of such processing is shown in Fig. 6 and includes austenization at 1150 °C, air cooling (at a speed of ≈1 °C/s) to the rolling temperature, rolling by ≈25%, quenching from the rolling temperature into water and subsequent tempering above the rolling temperature.

The temperature of warm rolling should be higher than the start temperature of the martensitic transformation M_s, while it is necessary to avoid falling into the temperature region of ferrite stability, in which austenite turns into ferrite during slow cooling. On the other hand, this temperature should be low enough to prevent intensive annihilation of dislocations during recrystallization or return. In work [57], based on calculations in the MatCalc program, it was established that the rolling temperature should be in the range between 600 °C and 700 °C or near 800 °C. The temperature of the final tempering should not be lower than 650 °C, *i.e.*, the expected operating temperature of the steel [57].

In the state after austenization at 1150 °C, rolling at 600 °C and quenching in water of Grade 9 steel, a highly defective martensitic structure with *MX* particles ranging in size from 10 to 150 nm is observed (90% of these particles have sizes <50 nm). According to the authors [57], they are not formed during rolling, but are Nb(C,N) particles that have not dissolved during austenization.

As a result of thermomechanical processing of Grade 91 steel (warm rolling + tempering), firstly, the grinding of the martensite structure

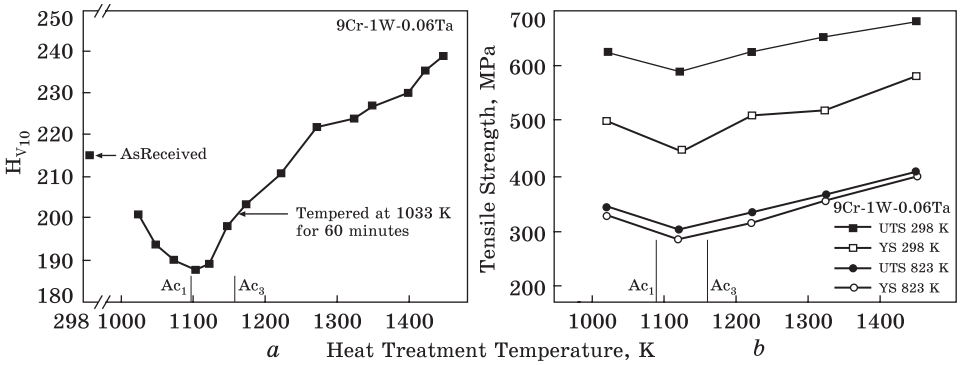

Fig. 7. Change in microhardness (*a*), yield strength and strength (*b*) of 9Cr–1.0W–0.6Ta steel depending on the heating temperature for quenching [51]

occurs compared to the state after traditional heat treatment, *i.e.*, the width of the martensite plates decreases by ≈1.7 times, namely, 210 nm after thermomechanical treatment (TMT) and 370 nm after THT; secondly, the average size decreases several times *MX* particles (10 nm after TMT, 50 nm after THT). The dimensions of $M_{23}C_6$ carbides after thermomechanical treatment are of 100–200 nm [57–59].

Thus, thermomechanical processing is an effective way to control the characteristics of the defective and heterophase structure of high-chromium ferritic–martensitic steels. With the help of properly selected TMT modes for steels of this elemental composition, it is possible to increase significantly the density of dislocations and the stable *MX* particles that effectively fix them.

According to Refs. [54, 60], by controlling the parameters of thermal or thermomechanical treatment of ferritic–martensitic steels, it is possible to significantly modify their structural–phase state and control the contribution of various factors to hardening at different temperatures.

In work [51], using the example of 9Cr–1.0W–0.6Ta steel, it was shown that both the microhardness value and the yield strength and strength limits of ferritic–martensitic steels largely depend on the austenization temperature (Fig. 7). The higher the temperature of heating for quenching, the higher these characteristics are. The decrease in hardness and strength during quenching from the intercritical temperature range (A_{c3}–A_{c1}) is typical for 9% Cr steels and is associated, firstly, with a decrease in the density of dislocations in martensite and the formation of ferrite grains and, secondly, with the enlargement of $M_{23}C_6$ and *MX* particles. With an increase in the austenization temperature above A_{c3}, the dissolution of the carbide phase particles begins, as a result, the austenite enriched with carbide-forming elements turns into martensite at a lower temperature. It is known that the greater the

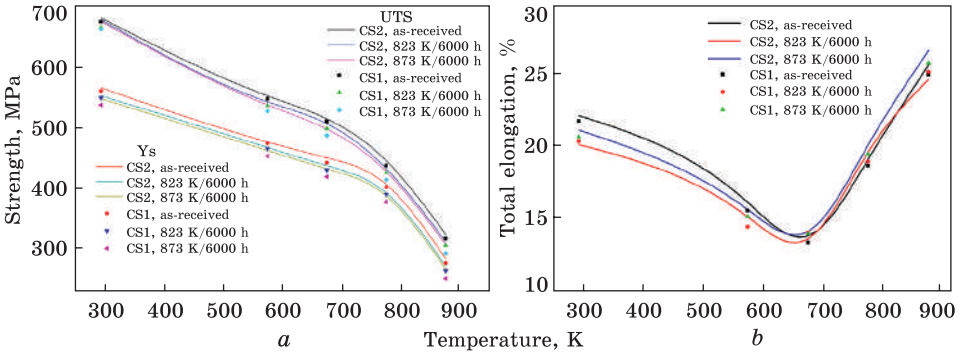

Fig. 8. The effect of prolonged annealing on the tensile mechanical properties of 9% Cr ferrite–martensitic steel CLF-1 [62]

austenite supercooling degree, the more dispersed and durable martensite is formed. The authors of Ref. [51] also showed that the grain size of the former austenite has a negligible effect on the characteristics of short-term strength. To a much greater extent, they are controlled by the size of martensitic lamellae, which are smaller the higher the quenching temperature. Abe and Nakazawa [61] also emphasize the important role of the size of martensitic plates and rails in combination with a high density of dislocations and fine particles anchoring them.

In work [62], the effect of prolonged (6000 h) annealing at temperatures of 550 and 600 °C on the microstructure and mechanical properties of poorly activated ferritic–martensitic 9% Cr CLF-1 steel was investigated. Such annealing does not significantly affect the size of ferrite grains, the width of martensitic lamellae and the dislocations density; however, it leads to enlargement (from 65 to 85 nm after annealing at 550 °C and up to 115 nm after annealing at 600 °C) of $M_{23}C_6$ carbides and their accumulation along the boundaries of martensite plates and grains of former austenite. At the same time, there is no noticeable increase in the size and volume fraction of *MX* carbonitrides. These changes in the microstructure of CLF-1 steel have little effect on its short-term mechanical properties. As can be seen from Fig. 8, prolonged annealing at 550 and 600 °C for 6000 hours does not lead to significant degradation of the characteristics of short-term strength and ductility of steel. This behaviour indicates a high thermal stability of its microstructure and, accordingly, mechanical properties at temperatures of 550 and 600 °C [62].

In works [63, 64], the effect of prolonged (up to 100,000 h) high-temperature annealing in the temperature range of 300–650 °C on the microstructure and mechanical properties of 9% ferritic–martensitic steel F82H was investigated. Prolonged annealing of this steel can lead to the return of the martensitic structure, the enlargement of carbides

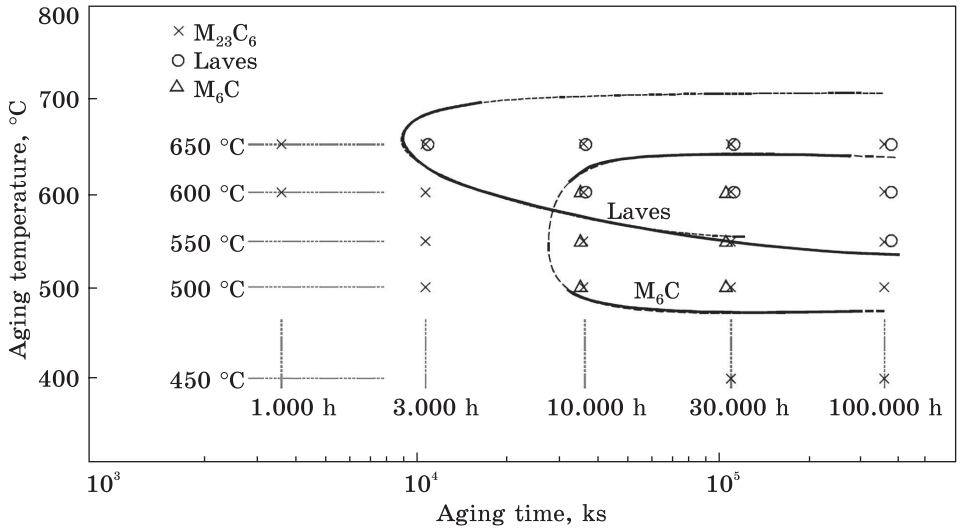

Fig. 9. Effect of annealing temperature on the carbide subsystem of F82H steel [63]

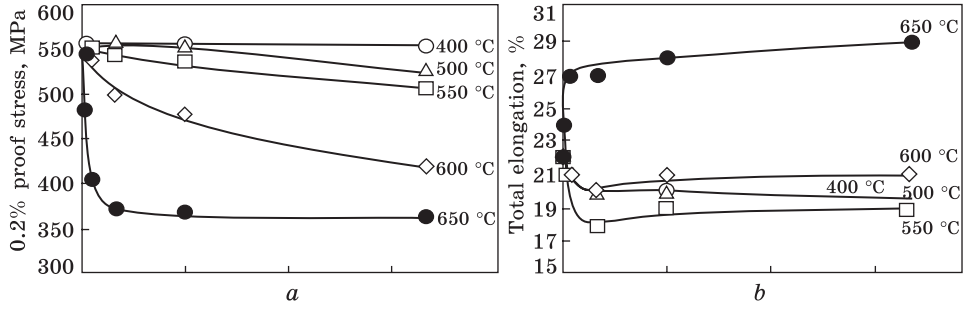

Fig. 10. Mechanical tensile properties of F82H steel at 20 °C: yield strength (*a*) and total elongation (*b*) [63]

$M_{23}C_6$, the release of Laves phase particles (Fe_2W) and carbides M_6C. It is shown [64] that annealing for 5000 h in the temperature range of 300–600 °C does not lead to significant changes in the microstructure of this steel. The main difference between the initial and aged state is an increase in the volume fraction of particles of the second phases (mainly $M_{23}C_6$ carbides and Fe_2W type intermetallides) from 1.5% to 2.6% after annealing at 400–550 °C and up to 4.1% after annealing at 600 °C. At the same time, there is an increase in the average size of $M_{23}C_6$ carbides from ≈80 to 300 nm, and the particle sizes of *MX* remain unchanged. After exposure of 1000 hours at T = 600 °C and 650 °C and 100,000 h at 550 °C, Laves phase particles are isolated (Fig. 9) [63]. The results deserving attention are obtained in Refs. [65–67]. M_6C carbides in F82H steel are released at temperatures of 500–600 °C after exposure for 10,000 hours (Fig. 9) [63].

The effect of annealing in the temperature range of 400–550 °C on the mechanical properties of F82H steel is insignificant even after exposure for 100,000 hours. As seen from Fig. 10, *a*, annealing at temperatures < 550 °C does not lead to significant softening of the material. On the contrary, the separation and enlargement of the particles of the second phases causes degradation of plastic properties, but this process reaches saturation after 30,000 hours. Figure 10 also shows that the yield strength of F82H steel at ambient temperature decreases rapidly after prolonged annealing at $T \geq 600$ °C. The total elongation at the same time (ageing at 650 °C) increases markedly simultaneously with a decrease in strength. According to Ref. [63], this behaviour is associated with an intensive return of the martensitic structure.

The authors of Refs. [68, 69] believe that the microstructure stability of 9–12% Cr steels is mainly determined by the stability of the second phase emissions. It is known that $M_{23}C_6$ carbides and Laves phase particles fix the boundaries of martensitic lamellae and initial austenite grains, and nanoscale *MX*-type carbonitride particles fix dislocations inside the matrix grains. Sufficiently rapid enlargement of the secretions of the $M_{23}C_6$ phase and the particles of the Laves phase reduces their fixing effect, leading to an accelerated return of the martensitic structure.

As the results of numerous studies [70, 71] show, particles of the *MX* type have the greatest stability at temperatures ≥650 °C (even at an exposure time 100,000 h). However, according to Ref. [58], in steels containing niobium and at least 10% chromium, *MX* carbonitrides can dissolve when *z*-phase nitrides (Cr(Nb,V)N) are isolated. It was shown in Ref. [71] that the stability (tendency to dissolution) of fine particles of *MX* under the influence of high temperatures (and stresses) is determined by their shape and size. With equal longitudinal dimensions (*e.g.*, 8–10 nm), globular particles are more resistant to dissolution than plate-shaped particles. At the same time, an increase in the size of the latter to about 20×10 nm^2 restrains their noticeable dissolution both in creep tests and under the influence of radiation exposure [71].

It should be noted that a similar effect on the microstructure and mechanical properties is also observed during annealing of 9–12% Cr ferritic–martensitic steels EUROFER-97, CLAM, JLF-1 and others [72–76]. The features of the microstructure evolution in the prolonged ageing process are largely determined by the initial structural state. The above results also show that there is a correlation between the mechanical properties of the original and aged sample. Consequently, knowledge of the initial short-term mechanical properties of steels makes it possible to predict these properties after prolonged high-temperature exposure.

To assess the heat resistance degree, such characteristics as the limit of long-term strength and the time to failure at a certain tempera-

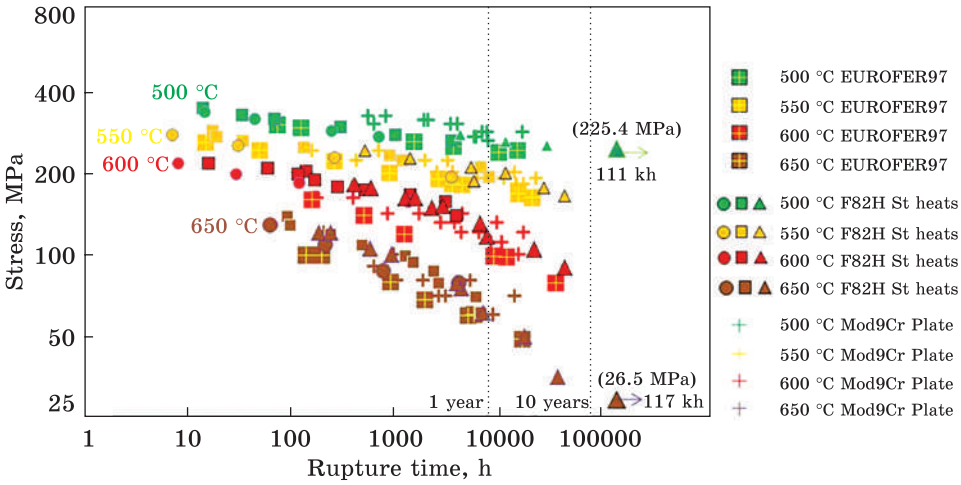

Fig. 11. Time to fracture during creep of F82H, EUROFER-97, and Mod9Cr–1Mo (T91) steels at different temperatures [77]

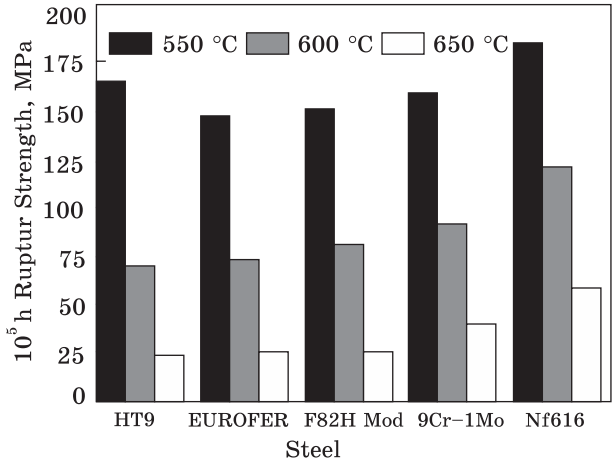

Fig. 12. Comparison of the long-term strength limits (at 100,000 h) of Sandvik HT9, EUROFER97, F82H, Mod9Cr–1Mo and NF616 steels at 550 °C, 600 °C, and 650 °C [38]

ture and stress are often used. Experimentally, they are determined by creep curves, *i.e.*, the dependence of deformation on time at given stresses and temperatures. Figures 11 and 12 show the results of tests for the high-temperature creep of some promising 9–12% Cr ferritic–martensitic steels [77]. From these figures, it can be seen that the long-term strength limit of F82H steel is comparable to that of Mod9Cr–1Mo steel, widely used in thermal power engineering. On the other hand, at high temperatures, F82H has some advantage over EUROFER-97 steel. The authors [77] attribute this difference to a higher W content in F82H steel.

According to Refs. [36, 38, 67, 69, 78, 79], the achieved heat resistance level of considered steels is ensured by the combined action of

substructural (grain and subgrain boundaries, high dislocation density), solid-solution and dispersion hardening ($M_{23}C_6$ carbides and MX carbonitrides). It is known that the creep rate and the time to fracture of steels at high temperatures control the return of the dislocation substructure. Therefore, to improve the creep characteristics of high-chromium ferritic–martensitic steels, it is necessary to increase the number of obstacles to the movement of dislocations, namely, the formation of a highly defective subgrain structure fixed by particles of the second phases.

At the same time, carbides $M_{23}C_6$ and thermally stable carbonitrides of the MX type are considered as hardening phases, as is shown in many works [1, 5, 29, 36, 38, 67, 69, 78, 79]. Laves phase and z-phase particles are undesirable. Due to the high rate of growth and coagulation, they do not provide the necessary level of long-term strength at high operating temperatures [80].

4. Features of Martensite Plastic Deformation Processes

Plastic deformation, as a rule, proceeds heterogeneously. The heterogeneity of plastic deformation can manifest itself on a different scale and for various reasons. In the course of technological processes, under conditions of complex deformation, various types of dislocation substructures are formed in the metal. At the same time, it is necessary to take into account that during plastic deformation, the defective substructure also evolves [81–83], various defects and their complex formations appear and disappear in the bulk of the deformed material, the structure parameters of the remaining defects change, and therefore knowledge of the nature and laws of the defective substructure evolution is necessary as well as diagnostic of defects [84, 85] and their distribution, including substitutional or interstitial atoms and vacancies [86–89]. The authors of work [13], studying the evolution of the defective substructure under large plastic deformations of the alloy by torsion on Bridgman anvils, believe that an important feature of the defective substructure at the first deformation stage, as in the case of rolling deformation, is the high density of submicrocrystals with high continuous misorientations or high density of boundaries with variable misorientation vectors modelled by clusters of continuously distributed partial one-sign disclinations. This type of substructure has been found to date in a wide class of submicrocrystalline materials: copper, nickel, *etc*. Sources of inhomogeneous stresses leading to the formation of substructures with a high curvature of the crystal lattice can be both dislocation ensembles with a high excess dislocation density of one sign, and the accumulation of continuously distributed partial disclinations in the boundaries with variable disorientation vectors [13].

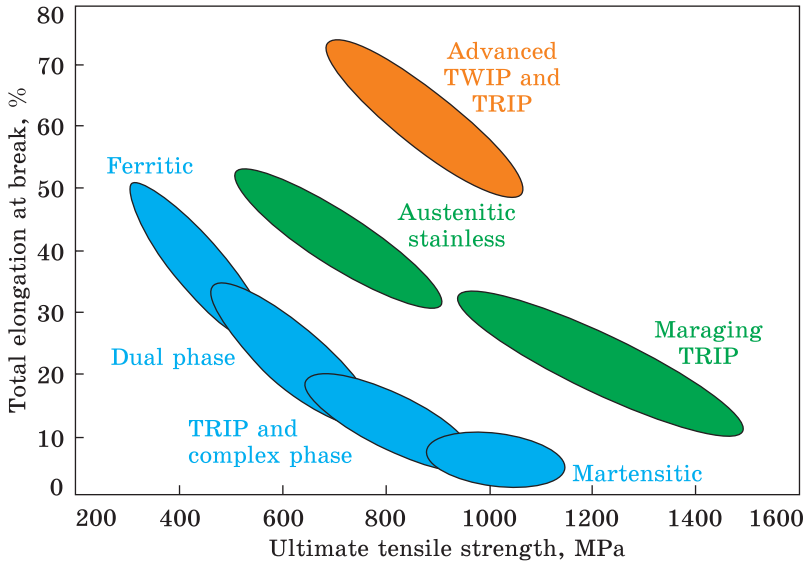

Fig. 13. Overview of typical strength–ductility profiles of different types of steels, indicating an inverse relation between these two properties [92]

Studying the dislocation substructure evolution of low- and medium-carbon steels during drawing [90, 91], it was found that as the deformation degree increases, in the studied steels the main chain of structural transformations in the dislocation ensemble is as follows: chaos→grids→cells→anisotropic fragments→isotropic fragments. An increase in the total deformation degree is accompanied by the development of the fragmentation process, and the volume fraction of the fragmented substructure increases almost linearly with an increase in the true deformation. This process is caused by the relaxation of long-range stress fields and self-organization of the dislocation substructure. The volume fractions of substructures change along the wire cross section in such a way that their evolution is closer to completion in the central zone. The scalar dislocation density and the torsion curvature of the crystal lattice increase, and the size of the cells and fragments decreases as they approach the centre of the sample. An increase in the drawing speed increases the scalar density of dislocations and creates a more uniform distribution of this characteristic over the cross section.

The study of the effects observed during phase transformations for plastic deformation made it possible to develop new classes of steels with plasticity induced by diffusion-free martensitic transformation. Such steels are called TRIP (transformation-induced plasticity) steels, and have one of the best strength indicators with a sufficiently high plasticity. Further investigation of the features of the course of marten-

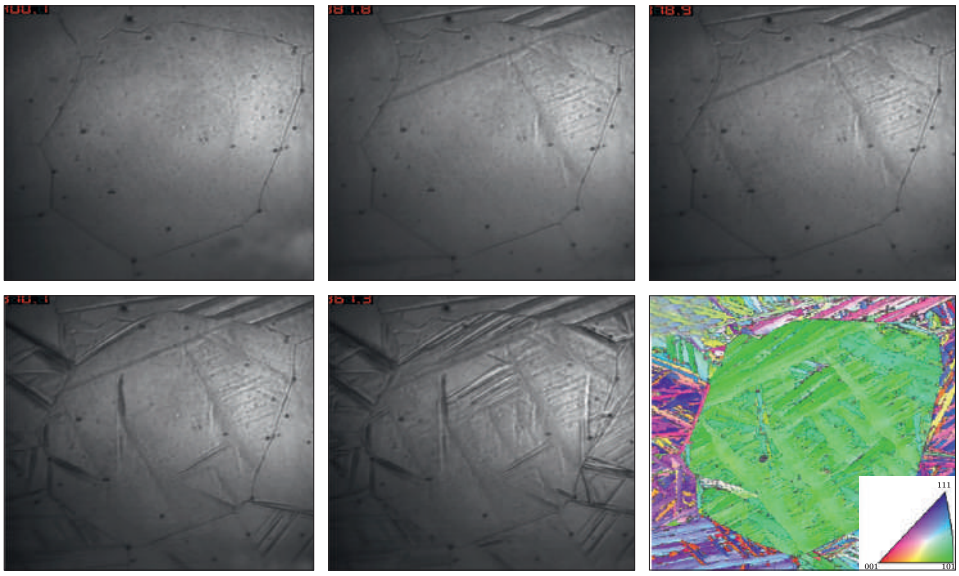

Fig. 14. The growth of martensitic crystals in austenite grain with a decrease in temperature from 400 to 360 °C and the corresponding map in the colours of the reverse pole figure [95]

sitic transformation at different temperatures made it possible to develop another class of high-strength steels with ductility induced by twinning, which became known as TWIP (twinning-induced plasticity) steels. They are characterized by high plasticity with good strength characteristics. Schematically, their position, indicated in the values of strength and ductility, compared with other classes of steels is shown in Fig. 13. As an example of the achievability of such mechanical properties, the work [86] can be noted, where the authors obtained a TRIP steel with a tensile strength of 1000 MPa and a relative elongation of 60%.

Recently, some authors [93, 94] have reported the creation of a new class of high-strength steels, called MBIP (microband-induced plasticity) steels, combining a combination of high strength properties of TRIP steels with excellent ductility indicators, which are inherent in TWIP steels.

The martensitic transformation occurring during cooling obeys the general laws of phase transformations occurring in the solid state. The thermodynamic stimulus in this case is the temperature, with a decrease in which it becomes more energetically advantageous to form a new phase. The formation process of martensitic crystals is considered in detail in Ref. [95], where their growth in a separate austenite grain was studied at a temperature drop from 400 °C to 360 °C (Fig. 14).

Historically, the largest number of studies has been devoted to the martensitic transformation occurring during the cooling of steels, which is considered in a number of monographs, *e.g.*, [96]. Later, it was ex-

perimentally proved that this transformation is one of the most common in solids and is observed in a variety of metals and alloys under different conditions. It was also found that for steels, the appearance of martensite is possible not only during cooling. Authors of Ref. [97] proposed to distinguish the following three types of martensite: cooling martensite, stress martensite, and strain martensite. Thus, the martensitic transformation can act in two forms: (i) as a phase transition of the first kind initiated by high-speed cooling and (ii) as a process occurring during deformation and initiated either by a given stress level (stress martensite) or a given strain level (strain martensite). As already mentioned, there are quite a lot of works in which the formation of cooling martensite is investigated, since quenching on martensite is one of the most important technological operations to increase the strength of manufactured products. Much less research has been conducted on the formation of martensite during deformation.

Authors of Refs. [98, 99] who studied the behaviour of metastable manganese-based steels, authors of Ref. [100] who studied high-strength steels with both martensitic transformation and twinning in the study of the strength properties of austenitic steels, authors of Ref. [101] who studied in detail the problems of fatigue of materials, including metastable steels, made a significant contribution to the study of the kinetics of martensitic transformation occurring during deformation.

For the first time, the appearance of martensite during deformation was noted in Ref. [102], where it was indicated that with a decrease in the temperature of the martensitic transformation below ambient temperature, plastic deformation could initiate a transition from γ (f.c.c.) to α' (b.c.c.) martensite. Moreover, the amount of formed martensite is directly proportional to the deformation degree.

The study of the stress martensite microstructure formed under the action of the applied load revealed its significant similarities with cooling martensite having a lamellar structure. It was noted that the martensite deformation structure is special: fine, rack-and-pinion, highly dispersed.

The martensite formed during deformation significantly improves the mechanical properties of the material. Steels undergoing this transformation during deformation show significantly greater elongation with similar strength characteristics than steel similar in chemical composition. In addition, such steels with equal elongation have increased tensile strength, compared with similar steels without martensitic transformation [103]. This is explained by the fact that deformation martensite has an increased dislocation density compared to cooling martensite. It promotes additional local hardening, which prevents the localization of plastic deformation in the neck, thereby distributing it over a larger area, which leads to a slowdown in destruction. For this reason,

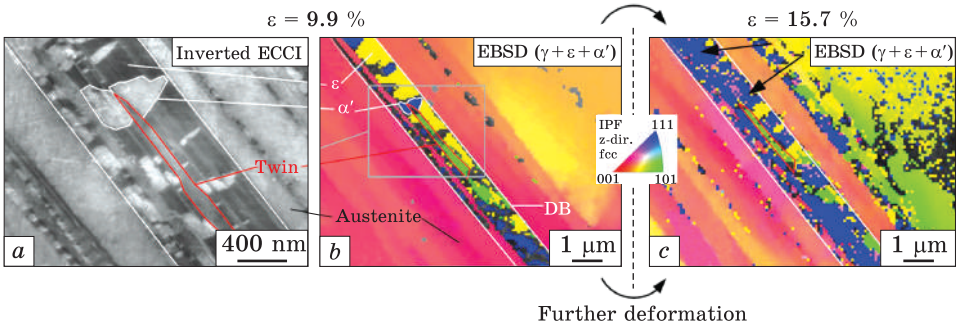

Fig. 15. Microstructure change according to the electron backscatter diffraction (EBSD) analysis for 16Cr6Mn6Ni steel deformed to elongation (*a*) 9.9% and (*b*) 15.7%: γ-austenite (f.c.c.) is shown in the colours of the reverse pole figure, yellow so-called ε-martensite (h.c.p.), blue α′-martensite and δ-ferrite (b.c.c.) [112]

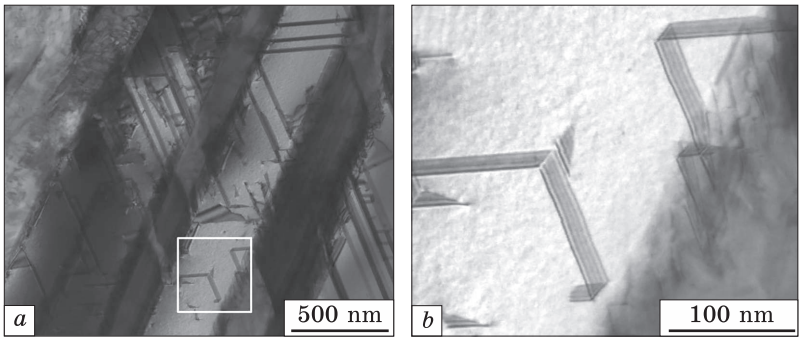

Fig. 16. Image obtained on a transmission electron microscope (TEM) of a prepared foil made of 16Cr6Mn6Ni steel after deformation to a relative elongation of 8%: deformation bands consisting of packaging defects (*a*) and individual packaging defects from different sliding systems (*b*) [112]

the materials with a similar effect are significantly superior to others, for example, in terms of impact strength.

To obtain high strength and ductility indices, it is necessary that the temperature, at which the metastable steel under study is deformed, be between the M_n and M_d points; this was shown for an alloy containing 29% of Ni and 0.26% of C in Ref. [104].

In addition, in order to obtain optimal physical and mechanical properties, the grain size is important, since the amount of deformation that must be applied to form crystals of the martensitic phase depends on it. Thus, in the work [105] on steel containing 0.1% C, 1.5% Mn, 0.5% Si, and 0.1% V, austenitic grains with a size of 2–6 microns turned into martensite faster than smaller ones.

The transformation process from γ (f.c.c.) to α′ (b.c.c.) can often proceed through an intermediate phase with an h.c.p. lattice, the so-

called ε-martensite, which was noticed by Schmidt during the x-ray analysis of Fe–Mn alloys. As calculated [106], often the transformation of the f.c.c. lattice into h.c.p. is energetically more advantageous than the transformation immediately into a b.c.c., since, in this case, only the order of laying of close-packed layers changes. The formation of an h.c.p. lattice can be considered as f.c.c. with packaging defects in one layer.

Later, the presence of this phase was also discovered and investigated in the works of other scientists [107]. Thus, for metastable steels, the process of converting austenite into other structures (phases) can proceed in three ways: $\gamma \rightarrow \varepsilon$, $\gamma \rightarrow \alpha'$, $\gamma \rightarrow \varepsilon \rightarrow \alpha'$, which has been well shown for Fe–Mn alloys with variable manganese content (see also effects of cyclic martensitic γ–ε and γ–ε–γ transformations on diffusion characteristics (of Co and C) in Fe–Mn-based alloys [108, 109]).

Studies of the features of the formation of the embryo of the martensitic phase were carried out in Ref. [110], where it was found on steel 18% Cr, 8% Ni that the embryo of the α' martensitic phase is formed at the junction of two series of dislocations. In the work [103] carried out on AISI 304 steel, the formation of a new phase embryo was detected at the intersection of packaging defects in the slip strip. A similar study of the ε and α' phases' formation was carried out in a work [112] for the Fe–Ni metastable steels (Fig. 15).

According to the data presented above, the intersection of deformation lines after the start of loading is the nuclei for the formation of ε-martensite with an h.c.p. lattice, which, with further deformation, transforms into α'-martensite. At the same time, using a high-resolution technique in a scanning electron microscope, the same authors showed that the h.c.p. structure of ε-martensite is formed by close stacking of lamellae of packaging defects (Fig. 16).

5. Features of Ultrafine-Grained State of Steels with Martensitic Structure

The properties of the obtained ultrafine-grained (UFG) materials largely depend on the method and conditions for obtaining UFG structures [113–119]. Now, there are two different approaches to obtaining bulk materials with nanoscale or ultrafine-grained structural elements. The first, the so-called 'bottom-up' one, in which the production of bulk blanks with nanostructured elements, is created by compacting powders with smaller nanostructured particles. Powders are obtained by grinding in a ball mill, gas condensation in an inert gas atmosphere, *etc*. However, bulk blanks at the same time have a number of disadvantages that limit their wide application, the main of which are high residual porosity (≈10%), small billet sizes and high chemical heterogeneity [120, 121].

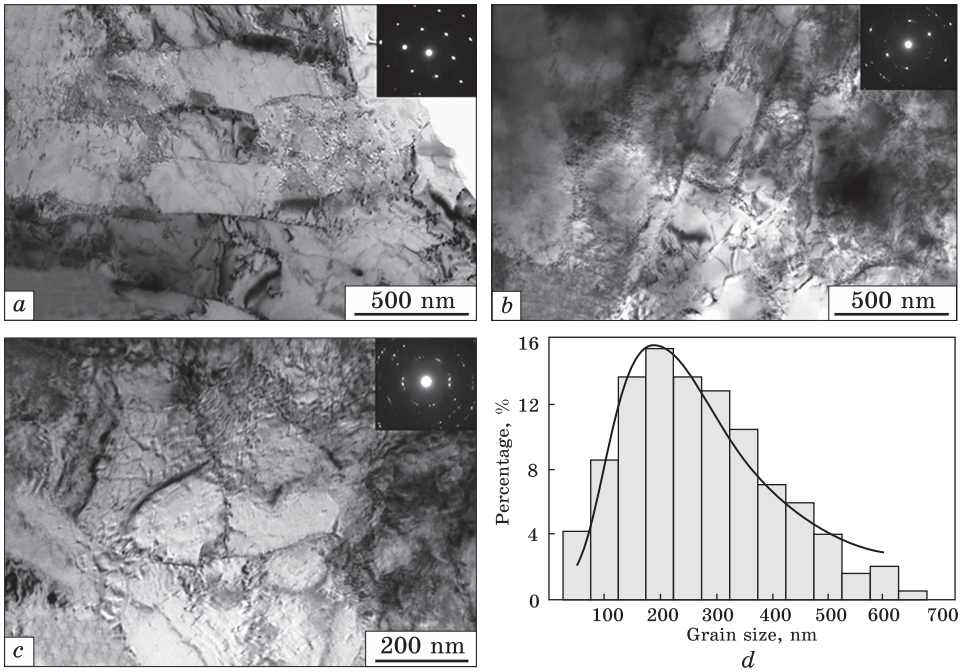

Fig. 17. TEM micrographs of 9% Cr steel: initial sample (*a*); one pass of ECAP (*b*); six ECAP passes (*c*); histogram of grain distribution after 6 ECAP passes (*d*) [131]

The use of the 'top–down' approach, when large deformation degrees are applied to the samples at low temperatures, as well as the possibility of using various deformation schemes, avoids the disadvantages inherent in the 'bottom-up' approach [122]. The most common and studied methods of severe plastic deformation are high-pressure torsion and equal-channel angular pressing. A high level of properties when using these methods is provided by the formation of structures with nanoscale elements, high-angle misorientation, high dislocation density and non-equilibrium grain boundaries [123–126]. Other methods also related to severe plastic deformation are comprehensive forging [127] and screw extrusion [128].

Structure formation in the severe plastic deformation (SPD) process proceeds in several stages, which are well studied on various metallic materials [9, 129, 130]. At the first stage, there is an increase in the dislocations density, the formation of a cellular and fragmented structure. At low deformation degrees, the misorientation angles of grain boundaries are less than 1°. With a further deformation degree increase, the misorientation angle of grain boundaries increases, the grain size decreases, and the cellular structure is formed. Microstrips and shear bands are formed, the misorientation angle of grain boundaries increases, which leads to the formation of a grain structure, mainly with high-

angle misorientations (≥6°). Thus, in Ref. [131], the use of the equal-channel angular pressing (ECAP) for steel with a 9% Cr content made it possible to grind the structure from 20 microns in the initial state to 200 nm after 6 passes at room temperature. Figure 17 shows the microstructure evolution during ECAP after 1 and 6 passes. This treatment led to an increase in microhardness from 2.7 GPa in the initial state to 3.8 GPa after 6 passes, the tensile strength increased from 730 to and 1160 MPa, and elongation decreased from 23 to 10%, respectively.

As is known, the nanocrystalline and UFG states formed during the SPD process are metastable, and when heated, properties are lost due to the transition to a large-crystalline state. Studies on pure metals, including in α-Fe, have shown the beginning of grain growth at $T/T_{\text{melt}} \leq$ $\leq$ 0.4 [132]. The authors of Ref. [133] conducted a study of thermal stability during annealing of submicrocrystalline (SMC) low-carbon steels (10G2FT and 06MBF), depending on the initial structural–phase state, which were obtained by varying the temperature and number of passes in the ECAP process. In the initial state, the steels contain carbides MC, M_3C, $M_{23}C_6$. Annealing in the temperature range of 300–700 °C showed the stability of microstructures up to 500 °C, regardless of the structural–phase state up to ECAP. After annealing at 600 °C, differences in the initial structural–phase state appear. Thus, in samples with the initial pearlite structure, the processes of collective recrystallization begin, and the structure becomes microcrystalline. Annealing of SMC structures, which had the structure of martensite and ferrite before ECAP, have a similar character of the kinetics of grain growth, but retain the SMC character. Annealing at 700 °C leads such a structure to microcrystalline dimensions.

High-alloyed martensitic steels are difficult to deform due to high alloying and the presence of carbide particles providing high strength properties. Thus, in Ref. [134], after one ECAP pass at ambient temperature in heat-resistant martensitic steel (15% Cr), the initial martensitic plates are grinded, inside which the dislocation grids are formed and dislocation density increases. Carbide particles acquire an equiaxial shape. During the subsequent ageing, the particles partially dissolve and their distribution is more uniform. At the same time, there is a simultaneous increase in strength and plasticity, due to the grinding of grain and a more uniform particles distribution.

The influence of alloying elements on the level of properties obtained in ECAP, such as Mo, Ti, V, Nb, which are carbide-forming agents, was studied in Ref. [135]. A submicrocrystalline structure with an average size of structural elements of 325 nm was formed in low-carbon steel 06MBF after 4 passes ECAP at 300 °C. At the same time, due to an increase in particle dispersion, density of their distribution, grain grinding and an increase in dislocation density, the yield strength

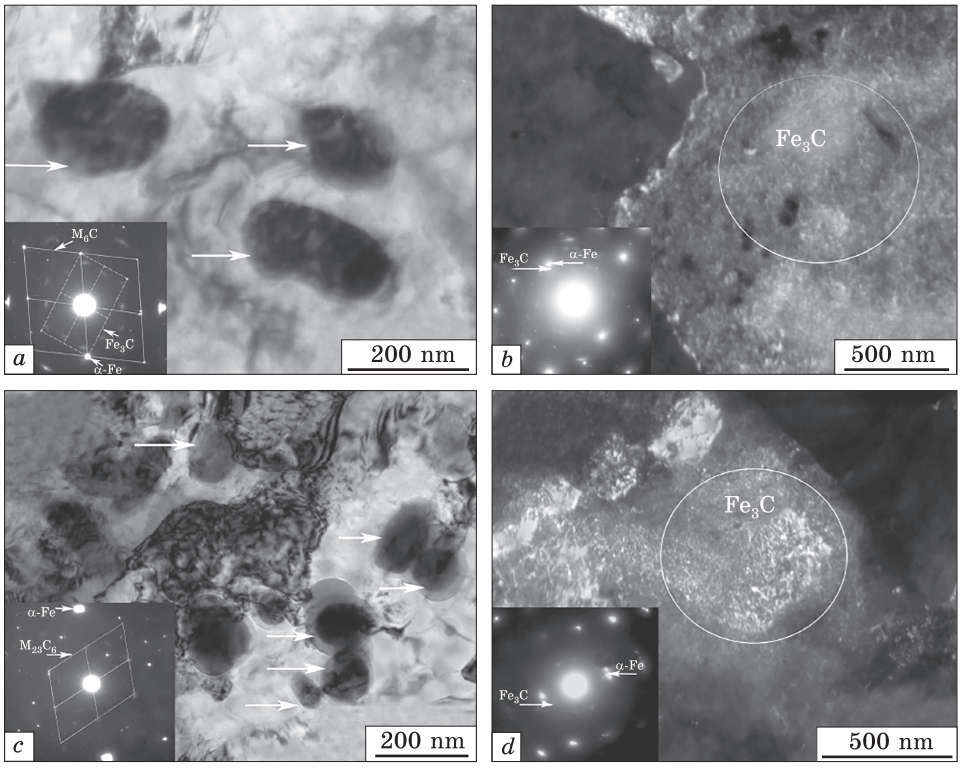

Fig. 18. TEM images of carbides M_6C, Fe_3C, and $M_{23}C_6$ in ferrite steel 06MBF: in the initial state (*a*, *b*) and after ECAP (*c*, *d*) [133]

increased from 480 to 815 MPa, plasticity was 5%. Figure 18 shows TEM images of steel, which clearly show the grinding of carbide particles.

In work [136], metastable austenitic stainless steel SUS304 was investigated after high-pressure torsion at ambient temperature after various anvil rotation speeds. The initial state of the steel was obtained by annealing at 1100 °C for 1 hour, followed by quenching in ice water. The prepared samples for high-pressure torsion had 10 mm in diameter and 0.85 mm in thickness. HPT was carried out under an applied pressure of 5 GPa. The number of revolutions varied from 0.03 to 50 at an anvil rotation speed of 0.2 and 5 revolutions per minute.

After HPT at rotation speed of 0.2 revolutions per minute at the early stage of deformation, the volume fraction of austenite decreases, and the volume fraction of α′-martensite and ε-martensite increases rapidly. For example, after 0.03 revolutions, the volume fraction of ε-martensite reaches 11%, but with a further increase in the number of revolutions to 0.25, the content of ε-martensite decreases and it completely disappears. The volume fraction of α′-martensite continues to increase and, after 0.5 turns, ≈100% is formed, and with further defor-

mation remains almost unchanged. HPT at rotation speed of 5 revolutions per minute leads to a rapid decrease in the volume fraction of austenite, and, at 0.25 revolutions, it reaches a minimum value of 15%. At the same time, the content of α′-martensite is 79%, and the content of ε-martensite is 6%. Further, deformation leads to an increase in the volume fraction of austenite and, consequently, a decrease in the content of α′- and ε-martensite. This indicates that during HPT at high rotation speed, not only direct (γ→α′), but also inverse (α′→γ)-martensitic transformations are realized [136].

In work [137], metastable austenitic steel 03H14N11K5M2YUT was studied after applying the following methods of severe plastic deformation: equal-channel angular pressing, drawing and high-pressure torsion. This steel was developed by the authors, since metastable austenitic steels (12X18H10T, *etc.*) currently used in industry have low strength properties at temperatures above 300 °C and under particularly hard loading conditions, these indicators are insufficient for them. In this regard, the authors conducted a study of austenitic steel 03X14N11K5M2YUT at $T > 300$ °C.

Equal-channel angular pressing was carried out in 4 and 6 passes at a temperature 325 °C for samples with a diameter of 10 mm and a length of 60 mm. After ECAP, there is an increased dislocation density and a predominantly submicrocrystalline structure. In addition, the samples showed a 2–3-fold increase in strength properties with a slight decrease in plasticity. This state is characterized by a microstructure with an average grain size of 50–100 nm. The authors have shown that (γ→ε→α′) and (γ→α′) transformations occur after ECAP at 4 and 6 passes. As a result, the maximum volume fraction of α′-martensite reaches 50% after 6 ECAP passes [137].

In the process of cold drawing [137], an axial structure is formed for samples with a diameter of 8 mm. At the deformation degree $e = 0.52$, numerous packing defects, deformation twins and ε-martensite are observed in the structure. Deformation at $e \approx 4$ leads to an increase in the volume fraction of α′-martensite to 98%. At the same time, the grain sizes of α′-martensite are of ≈50 nm. The formation of such a structure makes it possible to increase the strength properties of steel by 3–4 times.

In work [138], the influence of thermomechanical treatment parameters on the features of the nanocrystalline structure in austenitic steel AISI 301 was studied. In the initial state, the average grain size is of ≈18 microns. Cold rolling was carried out in the temperature from –196 °C to 0 °C with a strain rate of 0.5 s^{-1}. Thermomechanical treatment was carried out, as shown in Fig. 5, in four stages:

(a) cold rolling at –10 °C with a deformation degree of 35%;

(b) subsequent annealing at 750 °C for 10 minutes;

(c) cold rolling at –10 °C with a deformation degree of 60%;

(d) subsequent annealing in the temperature range 600–850 °C for 30 seconds to 50 minutes.

During rolling at 0 °C, the volume fraction of α′-martensite reaches 100% with a deformation degree of 50%. However, rolling at –196 °C makes it possible to achieve 100% α′-phase at 20% deformation. According to the authors, the decrease in the necessary deformation with a decrease in temperature for the formation of a larger amount of α′-martensite is explained by a decrease in the energy of the packaging defect and an increase in the available chemical driving force for the transformation [138].

After the second stage, the microstructure consisted of 85% austenite with an average grain size of 3 ± 0.5 microns. The study of the microstructure after the fourth stage showed that a higher annealing temperature leads to a greater return of austenite with a short annealing time. Metastable austenitic steel AISI 304L after cold rolling was investigated in Ref. [139]. The initial state was obtained by annealing at 1080 °C for 1 hour, followed by cooling in water. Cold rolling was carried out in a two-roll rolling mill in several passes with a total deformation degree of 90%. The cold-rolled samples having a thickness of 1 mm were annealed at 825 °C for 30 seconds. Annealing was carried out from 2 to 8 cycles, followed by quenching in water after each cycle. In addition, annealing with a duration equal to the total time from all short annealing cycles was studied to compare the effect on the microstructure.

Based on the results of calculating the required time for uniform temperature distribution over the sample during annealing, the authors of Ref. [140] note that 14–18 seconds at temperatures of 775–900 °C are sufficient for this. Therefore, the use of 30-second annealing is sufficient to equalize the temperature according to the sample. The estimated heating rate was 58 °C/s.

In the initial state, the microstructure is characterized by polygonal grains with an average size of about 85 ± 4 microns. Cold rolling leads to a general elongation of the grains in the direction of rolling. As a result, a fibrous structure is observed, which is stable after subsequent annealing at $T \leq 750$ °C for 5 minutes. However, annealing at 825 °C for 1 minute makes it possible to eliminate the fibrous structure [139].

It should be noted that in the process of cold deformation, a direct γ→α′-martensitic transformation is realized. The volume fraction of α′-martensite reaches 24.5%. Subsequent annealing of the samples leads to reverse martensitic transformation. The complete return of austenite is achieved by annealing within 5 minutes. A full return of austenite is also possible due to 10 cycles of 30 seconds, respectively [139].

The features of the structure after this thermomechanical treatment are submicrocrystalline austenitic grains ($d < 500$ nm) and areas

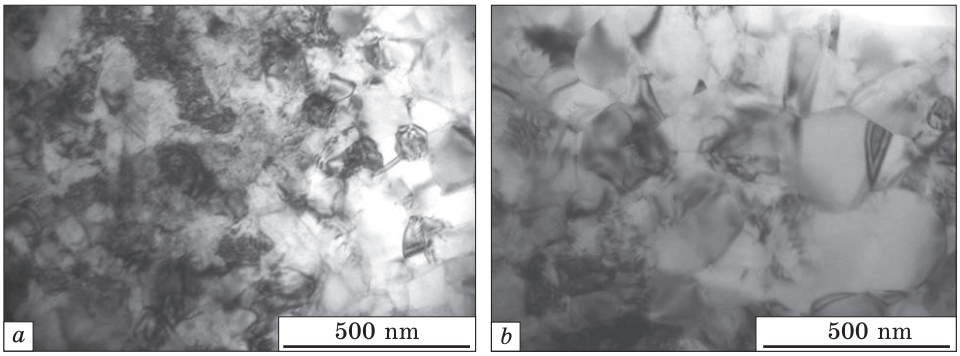

Fig. 19. Microstructure of AISI 304L steel after 4 annealing cycles at 825 °C [139]

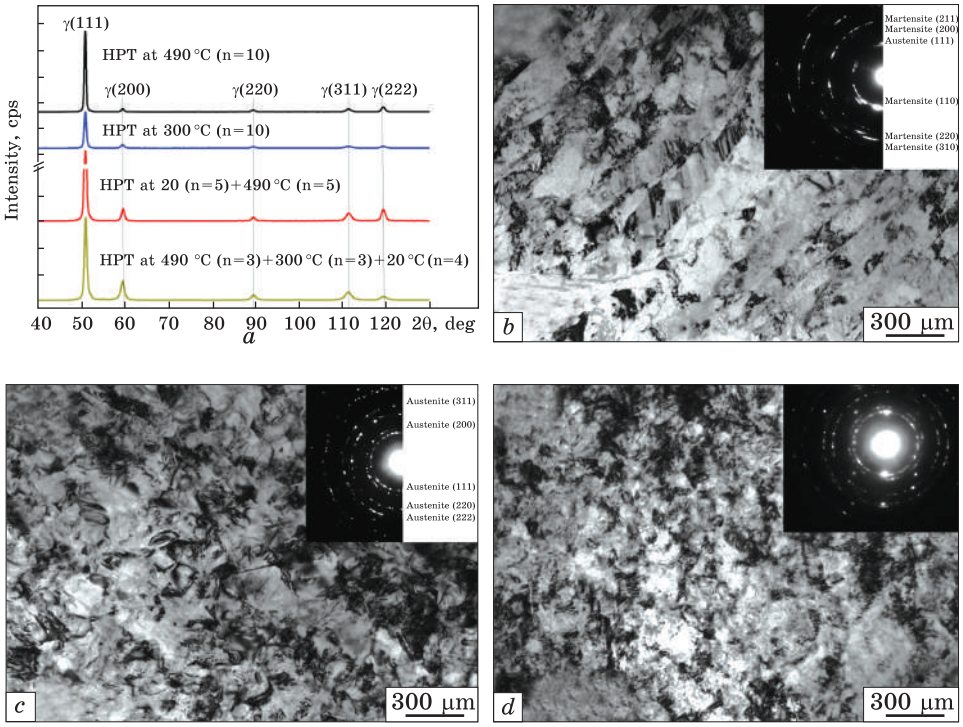

Fig. 20. The x-ray phase analysis of the steel produced by the high-pressure torsion (HPT) *via* different modes (*a*) and transmission electron microscopy observations for the HPT steel produced via modes 1 (*b*), 3 (*c*) and 5 (*d*) [141]

with high dislocation density. A reduction in the volume of such a microstructure formed after cold deformation is possible due to an increase in the number of short annealing cycles. At the same time, the grain size of austenite increases. Figure 19 shows a typical microstructure after 4 annealing cycles at 825 °C [139].

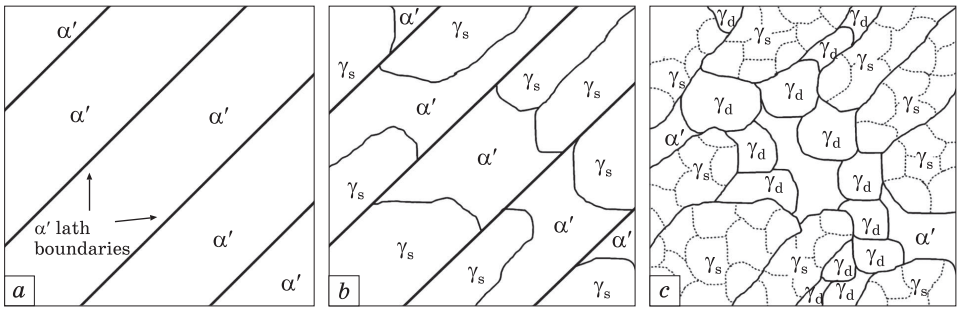

Fig. 21. Diagram of microstructural changes of the alloy during continuous heating and isothermal exposure: cold-rolled (*a*); during continuous heating (*b*); during isothermal exposure (*c*) [142]

In work [141], the metastable austenitic steel 08X18N10T was studied after HPT followed by annealing. The initial state was obtained by annealing at T = 1050 °C for 1 hour, followed by cooling into water. HPT under a pressure of 6 GPa was carried out: (i) at temperatures of 20 °C (mode 1), 300 °C (mode 2) and 450 °C (mode 3); (ii) with a step increase in the processing temperature from 20 °C to 450 °C (mode 4); (iii) with stepwise reduction of the processing temperature 450 °C → 300 °C → 20 °C (mode 5). The total number of revolutions was 10 for each processing mode. The samples after HPT had the shape of a disk with a diameter of 20 mm and 1 mm in thickness.

X-ray phase quantitative analysis showed that after mode 1, the volume fraction of α′-martensite is of ≈74%. In other processing modes, the completely austenitic structure is preserved. This is because the temperatures of 300 °C and 450 °C are much higher than the formation temperature of deformation martensite. Because of HPT, even in mode 4, the formed α′-martensite at 20 °C passes back to austenite with a further increase in temperature. For mode 5 with a decrease in temperature, the formation of a completely austenitic structure, according to the authors, is explained by the fact that grain grinding during deformation leads to a decrease in the temperature of M_s for the beginning of martensitic transformation [141].

After HPT at an applied pressure of 6 GPa and after mode 5, a nano- and submicrocrystalline structure with an average grain size of 60–120 nm is formed (Fig. 20) with increased strength properties [141].

In work [142], the reverse transformation of martensite into austenite in a metastable austenitic alloy during continuous heating with subsequent isothermal exposure was investigated. The initial state was obtained by quenching at 1200 °C for 12 hours, followed by hot deformation by rolling at 1000 °C with thinning to 10 mm. The obtained samples were subjected to cold rolling with a degree of deformation of 75%. As a result, cold deformation leads to an almost complete transformation

of austenite into martensite. This state is characterized by a lamellar α′-martensitic structure with an average lamella size of ≈200 nm (Fig. 21, *a*). The diffusion-free reverse (α′→γ)-martensitic transformation occurs during continuous heating to 520 °C at holding times of 30 seconds, 10 minutes and 30 minutes, respectively. During heating to 520 °C at a rate of 10 °C/s, the formation of 70% austenite is observed. As shown in Fig. 21, *b*, the microstructure after heating to 520 °C can be represented by a lamellar austenitic structure similar to the structure of martensite lamellae after cold rolling. In Figure 21, *b*, austenite formed by means of diffusion is designated as γ_s. The average size of austenitic lamellae is 100 nm [142].

A more complete reverse (α′→γ) transformation is possible after heating to 520 °C with subsequent isothermal exposure. At the same time, during isothermal exposure, the reverse transformation proceeds by diffusion, resulting in equiaxial austenite grains (Fig. 21, *c*). In Figure 21, *c*, austenite formed by means of diffusion is denoted as γ_d. With an increase in the exposure time to 30 minutes, a subgrain structure is formed in the austenite formed by means of diffusion. The dotted lines in Fig. 21, *c* show the boundaries of the subgrains. Thus, the formation of austenite during heating with subsequent isothermal exposure occurs both by diffusion-free and diffusion-free ways [142].

In work [137], the possibility of using low temperatures during rolling for the implementation of direct (γ→α′)-martensitic transformation was shown. In this regard, it is possible using the straight lines (γ→α)- and reverse (α→γ)-martensitic transformations during cooling and heating, to form submicrocrystalline and nanocrystalline states in metastable austenitic steels. Martensitic transformations during cooling (including to the boiling point of liquid nitrogen) are observed only in certain metastable austenitic steels having a sufficiently high start temperature of the martensitic transformation (M_s). At the same time, the use of plastic deformation after cooling contributes to a more intense (γ→α′)-martensitic transformation.

6. Conclusions

As can be seen from the literature review, a wide range of structural-phase states can be realized in ferritic–martensitic class steels, depending on their elemental composition and heat treatment conditions. In this regard, the solution of the above problems is associated, on the one hand, with the optimization of the elemental composition of steels, and, on the other hand, with the development of methods for modifying their microstructure.

Despite the considerable amount of work on the study of the microstructure features and mechanical properties of ferritic–martensitic

steels presented in the review of this work, many questions of the physics of the formation of microstructure and mechanical properties of these steels remain open. In our opinion, these are, firstly, the regularities of phase and structural transformations depending on the processing modes, for example, the influence of the quenching rate, temperature–time tempering regimes, and plastic deformation in the region of austenite existence on the features of the formation of heterophase and defective substructure, and others, and, secondly, the issues of the relationship of the microstructure of steels with their mechanical properties.

In addition, most of the works are devoted to adjustments of the elemental composition and optimization of the traditional processing mode (heating temperature for quenching, temperature and time of final tempering) of steels mainly with 9% chromium, as well as comprehensive certification of their microstructure and mechanical properties after this treatment. Only a small number of works are aimed at modifying their structural–phase state and mechanical properties using processing modes other than the traditional one.

The analysis of the literature data also shows that, despite the large amount of research on the influence of UFG structures on the microstructure and properties of various metallic materials, there is not enough data on the formation of UFG structures in ferritic–martensitic steels. At the same time, an urgent task is to increase the strength characteristics of steels of this class. A promising approach to solving this problem is the use of SPD methods, which allow achieving a high level of properties by grinding the grain structure, in combination with additional heat treatment.

REFERENCES

1. V.A. Lobodyuk and E.I. Estrin, *Martensitic Transformations* (Cambridge International Science Publishing: 2014).
2. N.A. Tereshchenko, I.L. Yakovleva, T.A. Zubkova, M.V. Chukin, and N.V. Koptseva, Structure levels of pearlite deformation in carbon steel of eutectoid composition, *Phys. Metals Metallogr.*, **114**: 430 (2013); https://doi.org/10.1134/s0031918x13050116
3. I.E. Volokitina, *J. Chem. Technol. Metall.*, 55, No. 2: 479 (2020).
4. A. Belyakov, T. Sakai, H. Miura, and R. Kaibyshev, Substructures and internal stresses developed under warm severe deformation of austenitic stainless steel, *Scr. Mater.*, **42**: 319 (1980); https://doi.org/10.1016/S1359-6462(99)00353-x
5. M.O. Vasylyev, B.M. Mordyuk, S.M. Voloshko, and D.A. Lesyk, Microstructure evolution of the carbon steels during surface severe plastic deformation, *Prog. Phys. Met.*, **22**, No. 4: 562 (2021); https://doi.org/10.15407/ufm.22.04.562
6. S. Lezhnev, E. Panin, and I. Volokitina, Research of combined process 'rolling–pressing' influence on the microstructure and mechanical properties of alumi-

nium, *Adv. Mater. Res.*, **814**: 68 (2013);
https://doi.org/10.4028/www.scientific.net/amr.814.68
7. M. Calcagnotto, Y. Adachi, D. Ponge, D. Raabe, Deformation and fracture mechanisms in fine- and ultrafine-grained ferrite/martensite dual-phase steels and the effect of aging, *Acta Mater.*, **59**: 658 (2011);
http://doi.org/10.1016/j.actamat.2010.10.002
8. A. Naizabekov and I. Volokitina, Influence of equal-channel angular pressing on changes in the microstructure of steel grade 1055, *Metallurgist*, **64**: 1029 (2021);
https://doi.org/10.1007/s11015-021-01083-3
9. R. Song, D. Ponge, D. Raabe, J. Speer, and D. Matlock, Overview of processing, microstructure and mechanical properties of ultrafine grained bcc steels, *Mater. Sci. Eng. A*, **441**: 1 (2006);
https://doi.org/10.1016/j.msea.2006.08.095
10. R. Song, D. Ponge, and D. Raabe, Mechanical properties of an ultrafine grained C–Mn steel processed by warm deformation and annealing, *Acta Mater.*, **53**: 4881 (2005);
https://doi.org/10.1016/j.actamat.2005.07.009
11. R. Song, D. Ponge, D. Raabe, and D. Kaspar, *Acta Mater.*, **53**: 845 (2005);
https://doi.org/10.1016/j.actamat.2004.10.051
12. A.V. Volokitin, I.E. Volokitina, and E.A. Panin, Thermomechanical treatment of stainless steel piston rings, *Prog. Phys. Met.*, **23**, No. 3: 411 (2022);
https://doi.org/10.15407/ufm.23.03.411
13. I.A. Ditenberg, A.N. Tyumentsev, K.V. Grinyaev, V.M. Chernov, M.M. Potapenko, and A.V. Korznikov, Features of the formation of the submicrocrystalline structural state upon plastic deformation of a V–4Ti–4Cr alloy in Bridgman anvils, *Technical Phys.*, **56**: 815 (2011);
https://doi.org/10.1134/s0031918x12020020
14. G. Krauss, *Metallurgical and Materials Transactions B*, **32**: 205 (2001);
https://doi.org/10.1007/s11663-001-0044-4
15. V.A. Lobodyuk, and E.I. Estrin, *Martensitnyye Prevrashcheniya* [Martensitic Transformations] (Moscow: FIZMATLIT: 2009) (in Russian).
16. A. Volokitin A. Naizabekov, I. Volokitina, S. Lezhnev, and E. Panin, *Mater. Lett.*, 304: 130598 (2021);
https://doi.org/10.1016/j.matlet.2021.130598
17. T.M. Radchenko, V.A. Tatarenko, Fe–Ni alloys at high pressures and temperatures: statistical thermodynamics and kinetics of the $L1_2$ or $D0_{19}$ atomic order, *Uspehi Fiziki Metallov*, **9**, No. 1: 1 (2008); https://doi.org/10.15407/ufm.09.01.001
18. T.M. Radchenko, V.A. Tatarenko, and S.M. Bokoch, Diffusivities and kinetics of short-range and long-range orderings in Ni–Fe permalloys, *Metallofiz. Noveishie Tekhnol.*, **28**, No. 12: 1699 (2006).
19. V.A. Tatarenko, S.M. Bokoch, V.M. Nadutov, T.M. Radchenko, and Y.B. Park, Semi-empirical parameterization of interatomic interactions and kinetics of the atomic ordering in Ni–Fe–C permalloys and elinvars, *Defect Diffus. Forum*, **280–281**: 29 (2008);
https://doi.org/10.4028/www.scientific.net/ddf.280-281.29
20. I.M. Melnyk, T.M. Radchenko, and V.A. Tatarenko, Semi-empirical parameterization of interatomic interactions, which is based on statistical-thermodynamic analysis of data on phase equilibriums in b.c.c.-Fe–Co alloy. I. Primary ordering, *Metallofiz. Noveishie Tekhnol.*, **32**, No. 9: 1191 (2010).
21. V.A. Tatarenko and T.M. Radchenko, The application of radiation diffuse scattering to the calculation of phase diagrams of f.c.c. substitutional alloys,

Intermetallics, **11**, Nos. 11–12: 1319 (2003);
https://doi.org/10.1016/s0966-9795(03)00174-2
22. T.M. Radchenko, V.A. Tatarenko, H. Zapolsky, and D. Blavette, Statistical-thermodynamic description of the order–disorder transformation of $D0_{19}$-type phase in Ti–Al alloy, *J. Alloys Compd.*, **452**, No. 1: 122 (2008);
https://doi.org/10.1016/j.jallcom.2006.12.149
23. T.M. Radchenko, V.A. Tatarenko, and H. Zapolsky, Statistical thermodynamics and ordering kinetics of $D0_{19}$-type phase: application of the models for h.c.p.-Ti–Al alloy, *Solid State Phenom.*, **138**: 283 (2008);
https://doi.org/10.4028/www.scientific.net/ssp.138.283
24. V.A. Tatarenko and T.M. Radchenko, Direct and indirect methods of the analysis of interatomic interaction and kinetics of a relaxation of the short-range order in close-packed substitutional (interstitial) solid solutions, *Usp. Fiz. Met.*, **3**, No. 2: 111 (2002);
https://doi.org/10.15407/ufm.03.02.111
25. T.M. Radchenko and V.A. Tatarenko, Atomic-ordering kinetics and diffusivities in Ni–Fe permalloy, *Defect Diffus. Forum*, **273–276**: 525 (2008);
https://doi.org/10.4028/www.scientific.net/ddf.273-276.525
26. S.M. Bokoch, M.P. Kulish, T.M. Radchenko, and V.A. Tatarenko, Kinetics of short-range ordering of substitutional solid solutions (according to data on a scattering of various kinds of waves). I. Microscopic parameters of migration of atoms within f.c.c.-Ni–Mo in Fourier-representation, *Metallofiz. Noveishie Tekhnol.*, **26**, No. 3: 387–406 (2004).
27. S.M. Bokoch, M.P. Kulish, V.A. Tatarenko, and T.M. Radchenko, Kinetics of short-range ordering of substitutional solid solutions (according to data on a scattering of various kinds of waves). II. Parameters of atomic microdiffusion within f.c.c.-Ni–Mo, *Metallofiz. Noveishie Tekhnol.*, **26**, No. 4: 541–558 (2004).
28. D.S. Leonov, T.M. Radchenko, V.A. Tatarenko, and Yu.A. Kunitsky, Kinetics parameters of atomic migration and diffuse scattering of radiations within the f.c.c.-Ni–Al alloys, *Defect Diffus. Forum*, **273–276**: 520 (2008);
https://doi.org/10.4028/www.scientific.net/ddf.273-276.520
29. M.A. Smirnov, V.M. Schastlivtsev, and L.G. Zhuravlev, *Osnovy Termicheskoy Obrabotki Staley* [Fundamentals of Heat Treatment of Steels] (Science and Technology: 2002) (in Russian).
30. Y.G. Andreev, B.G. Belyakov, and A.P. Gruzdov, Opredelenie Prostranstvennoy Formy i Razmerov Kristallov Martensita [Determination of Spatial Shape and Size of Martensite Crystals], *Fiz. Metal. Metalloved.* (1973) (in Russian).
31. V.I. Izotov, Morfologiya i Kristallogeometriya Reechnogo (Massivnogo) Martensita [Morphology and Crystallogeometry of Lath (Massive) Martensite], *Phys. Met. Metallurgy* (1972) (in Russian).
32. V.M. Schastlivtsev, Strukturnyye Osobennosti Martensita v Konstruktsionnykh Stalyakh [Structural Peculiarities of Martensite in Structural Steels], *Phys. Met. Metallurgy* (1972) (in Russian).
33. C.A. Apple, R.Y. Karon, and G. Kraus, Packet microstructure in Fe-0.2 pct C martensite, *Metallurgical Transactions*, **5**: 593 (2010);
https://doi.org/10.1007/bf02644654
34. Yu.G. Andreev, E.I. Zarkova, and M.A. Shtremel, Granitsy i Subgranitsy v Paketnom Martensite. I. Granitsy mezhdu Kristallami v Pakete [Boundaries and Subboundaries in Batch Martensite. I. Boundaries between Crystals in a Package], *Phys. Met. Metallurgy* (1990) (in Russian).

35. V.M. Schastivtsev, D.A. Mirzaev, and I.L. Yakovleva, *Strukturnye Osobennosti Martensita v Konstruktsionnykh Staliakh* [Structure of Heat-Treated Steel] (Metallurgy: 1994) (in Russian).
36. K. Maruyama, K. Sawada, and J. Koike, Strengthening mechanisms of creep resistant tempered martensitic steel, *ISIJ Int.*, **6**: 641 (2001); https://doi.org/10.2355/isijinternational.41.641
37. *Creep-Resistant Steels* (Eds. F. Abe, T.-U. Kern, and R. Viswanathan) (Elsevier–Woodhead Publishing: 2008)
38. R.L. Klueh, and A.T. Nelson, Ferritic/martensitic steels for next-generation reactors, *J. Nuclear Materials*, **371**: 37 (2007); https://doi.org/10.1016/j.jnucmat.2007.05.005
39. S. Raju, B. Ganesh, A. Rai, R. Mythili, S. Saroja, E. Mohandas, M. Vijayalakshmi, K.B.S. Rao, and B. Raj, Measurement of transformation temperatures and specific heat capacity of tungsten added reduced activation ferritic–martensitic steel, *J. Nuclear Materials*, **389**: 385 (2007); https://doi.org/10.1016/j.jnucmat.2009.02.030
40. H. Kitahara, R. Ueji, N. Tsuji, and Y. Minamino, Crystallographic features of lath martensite in low-carbon steel, *Acta Mater.*, **54**: 1279 (2006); https://doi.org/10.1016/j.actamat.2005.11.001
41. N.A. Polekhina, I.Yu. Litovchenko, and A.N. Tyumentsev, Vliyanie Temperatury Otpuska na Fazovyye Prevrashcheniya v Ferritno-Martensitnoy 12%-i Khromistoy Stali EK-181 [The Effect of Tempering Temperature on Phase Transformations in Ferritic–Martensitic 12% Chromium Steel EC-181], *VANT. Ser. Thermonuclear Synthesis* (2014) (in Russian).
42. D.R. Jara, 9–12% Cr Heat Resistant Steels: Alloy Design, TEM Characterization of Microstructure Evolution and Creep Response at 650 ˚C (Dissertation for Doctor of Engineering (Bochum: 2011).
43. K.A. Lanskaya, *Vysokokhromistye Zharoprochnye Stali* [High-Chromium Heat-Resistant Steels] (Metallurgy: 1967) (in Russian).
44. I.Yu. Litovchenko, N.A. Polekhina, and A.N. Tyumentsev, *Vliyanie Rezhimov Termoobrabotki na Mikrostrukturu i Mekhanicheskie Svoistva Zharoprochnoy Ferritno-Martensitnoy 12%-oy Khromistoy Stali EK-181* [Influence of Regimes of Heat Treatment on the Microstructure and Mechanical Properties of Heat-Resistant Ferritic–Martensitic 12% Chromium Steel EC-181], *VANT. Ser. Thermonuclear Synthesis* (2014) (in Russian).
45. R. Kaibyshev and I. Kazakulov, Deformation behaviour of Fe–3Si steel, *Mater. Sci. Technol.*, **20**: 221 (2004); https://doi.org/10.1179/026708304225010415
46. A.V. Dub, V.N. Skorobogatykh, and I.A. Shchenkova, New heat-resistant chromium steels for a promising objects of power engineering, *Therm. Eng.*, **55**: 594 (2008); https://doi.org/10.1134/s0040601508070124
47. J. Cadek, *Creep in Metallic Materials* (Prague: Academia: 1994).
48. J. Pilling and N. Ridley, *Superplasticity in Crystalline Solids* (London: The Institute of Metals: 1989), p. 214.
49. V.M. Chernov, M.V. Leont'eva-Smirnova, M.M. Potapenko, N.A. Polekhina, I.Yu. Litovchenko, A.N. Tyumentsev, E.G. Astafurova, and L.P. Khromova, Structure–phase transformations and physical properties of ferritic–martensitic 12% chromium steels EK-181 and ChS-139, *Tech. Phys.*, **61**: 97 (2016); https://doi.org/10.1134/s1063784216010084
50. I. Volokitina, E. Siziakova, R. Fediuk, and A. Kolesnikov, Development of a thermomechanical treatment mode for stainless-steel rings, *Materials* **15**, 4930

(2022);
https://doi.org/10.3390/ma15144930
51. K.S. Chandravathi, C.S. Sasmal, and K. Laha, Effect of isothermal heat treatment on microstructure and mechanical properties of reduced activation ferritic martensitic steel, *J. Nuclear Materials*, **435**: 128 (2013);
https://doi.org/10.1016/j.jnucmat.2012.12.042
52. R.L. Klueh, Elevated-temperature ferritic and martensitic steels and their application to future nuclear reactors (Oak Ridge National Laboratory: 2005);
https://doi.org/10.2172/885938
53. M.L. Bernstein and A.G. Rakhshtadt, *Metallovedenie i Termicheskaya Obrabotka Stali: Spravochnik* [Metallurgy and Heat Treatment of Steel: Handbook] (Metallurgy: 1983) (in Russian).
54. L. Tan, D. Hoelzer, J. Busby, M. Sokolov, and R. Klueh, Microstructure control for high strength 9Cr ferritic–martensitic steels, *J. Nuclear Mater.*, **422**: 45 (2012);
https://doi.org/10.1016/j.jnucmat.2011.12.011
55. I.E. Volokitina, Evolution of the microstructure and mechanical properties of copper under ECAP with intense cooling, *Metal Sci. Heat Treat.*, **62**, Nos. 3–4: 253 (2020);
https://doi.org/10.1007/s11041-020-00544-x
56. I.E. Volokitina, Effect of cryogenic cooling after ECAP on mechanical properties of aluminum alloy D16, *Metal Sci. Heat Treat.*, **61**, Nos. 3–4: 234 (2019);
https://doi.org/10.1007/s11041-019-00406-1
57. S. Hollner, B. Fournier, J. Pendu, T. Cozzika, I. Tourniй, J. Brachet, and A. Pineau, *Journal of Nuclear Materials*, **405**: 101 (2010);
https://doi.org/10.1016/j.jnucmat.2010.07.034
58. S. Lezhnev, A. Naizabekov, A. Volokitin, I. Volokitina, E. Panin, and M. Knapinski, *J. Chem. Technol. Metall.*, **52**: 172 (2017).
59. S. Hollner, E. Piozin, P. Mayr, C. Салs, I. Tourniй, A. Pineau, and B. Fournier, Characterization of a boron alloyed 9Cr3W3CoVNbBN steel and further improvement of its high-temperature mechanical properties by thermomechanical treatments, *J. Nuclear Mater.*, **441**: 15 (2013);
https://doi.org/10.1016/j.jnucmat.2013.05.018
60. R.L. Klueh, N. Hashimoto, and P.J. Maziasz, New nano-particle-strengthened ferritic/martensitic steels by conventional thermo-mechanical treatment, *J. Nuclear Mater.*, **367**: 48 (2007);
https://doi.org/10.1016/j.jnucmat.2007.03.001
61. F. Abe and S. Nakazawa, The effect of tungsten on creep behavior of tempered martensitic 9Cr steels, *Metall. Mater. Trans. A*, **23**: 3025 (1992);
https://doi.org/10.1007/bf02646120
62. P. Wang, J. Chen, H. Fu, S. Liu, X. Li, and Z. Xu, Effect of N on the precipitation behaviours of the reduced activation ferritic/martensitic steel CLF-1 after thermal ageing, *J. Nuclear Mater.*, **442**: 9 (2013);
https://doi.org/10.1016/j.jnucmat.2013.03.081
63. K. Shiba, H. Tanigawa, T. Hirose, H. Sakasegawa, and S. Jitsukawa, Long-term properties of reduced activation ferritic/martensitic steels for fusion reactor blanket system, *Fusion Engineering and Design*, **86**: 2895 (2011);
https://doi.org/10.1016/j.fusengdes.2011.06.005
64. J. Lapeca, M. García-Mazario, P. Fernández, and A.M. Lancha, Chemical segregation behavior under thermal aging of the low-activation F82H-modified steel, *J. Nuclear Mater.*, **283**: 662 (2011);
https://doi.org/10.1016/s0022-3115(00)00276-2

65. Z.M. Rykavets, J. Bouquerel, J.-B. Vogt, Z.A. Duriagina, V.V. Kulyk, T.L. Tepla, L.I. Bohun, and T.M. Kovbasyuk, Investigation of the microstructure and properties of TRIP 800 steel subjected to low-cycle fatigue, *Prog. Phys. Met.*, **20**, No. 4: 620 (2019);
https://doi.org/10.15407/ufm.20.04.620
66. A. Naizabekov, S. Lezhnev, E. Panin, and I. Volokitina, The role of preliminary heat treatment in the formation of ultrafine-grained structure in the implementation of the combined process 'rolling–equal channel angular pressing', *Mater. Sci. Forum*, **879**: 1093 (2016);
https://doi.org/10.4028/www.scientific.net/msf.879.1093
67. Q. Huang, N. Baluc, Y. Dai, S. Jitsukawa, A. Kimura, J. Konys, R. Kurtz, R. Lindau, T. Muroga, G. Odette, B. Raj, R. Stoller, L. Tan, H. Tanigawa, A. Tavassoli, T. Yamamoto, F. Wan, and Y. Wu, Recent progress of R&D activities on reduced activation ferritic/martensitic steels, *J. Nuclear Mater.*, **442**: 2 (2013);
https://doi.org/10.1016/j.jnucmat.2012.12.039
68. L. Huang, X. Hu, C. Yang, W. Yan, F. Xiao, Y. Shan, and K. Yang, Influence of thermal aging on microstructure and mechanical properties of CLAM steel, *J. Nuclear Mater.*, **443**: 479 (2013);
https://doi.org/10.1016/j.jnucmat.2013.08.008
69. J. Hald, Microstructure and long-term creep properties of 9–12% Cr steels, *J. Nuclear Mater.*, **85**: 30 (2008);
https://doi.org/10.1016/j.ijpvp.2007.06.010
70. Y.Z. Shen, S.H. Kim, C.H. Han, H.D. Cho, and W.S. Ryu, TEM investigations of MN nitride phases in a 9% chromium ferritic/martensitic steel with normalization conditions for nuclear reactors, *J. Nuclear Mater.*, **384**: 48 (2008);
https://doi.org/10.1016/j.jnucmat.2008.10.005
71. L. Tan T. Byun, Y. Katoh, and L. Snead, Stability of MX-type strengthening nanoprecipitates in ferritic steels under thermal aging, stress and ion irradiation, *Acta Mater.*, **71**: 11 (2014);
https://doi.org/10.1016/j.actamat.2014.03.015
72. Y.F. Li, T. Nagasaka, T. Muroga, Q.Y. Huang, and Y.C. Wu, Effect of thermal ageing on tensile and creep properties of JLF-1 and CLAM steels, *J. Nuclear Mater.*, **386**: 495 (2009);
https://doi.org/10.1016/j.jnucmat.2008.12.149
73. H. Hadraba, and I. Dlouhy, Effect of thermal ageing on the impact fracture behaviour of Eurofer'97 steel, *J. Nuclear Mater.*, **386**, 564 (2009);
https://doi.org/10.1016/j.jnucmat.2008.12.319
74. P. Fernández, M. Garcна-Mazario, A.M. Lancha, and J. Lapeca, Grain boundary microchemistry and metallurgical characterization of Eurofer'97 after simulated service conditions, *J. Nuclear Mater.*, **329**: 274 (2004);
https://doi.org/10.1016/j.jnucmat.2004.04.055
75. H. Sakasegawa, T. Hirose, A. Kohyama, Y. Katoh, T. Harada, K. Asakura, and T. Kumagai, Effects of precipitation morphology on toughness of reduced activation ferritic/martensitic steels, *J. Nuclear Mater.*, **307**: 490 (2002);
https://doi.org/10.1016/S0022-3115(02)01083-8
76. I. Volokitina, A. Volokitin, and D. Kuis, *J. Chem. Technol. Metall.*, **56**: 643 (2021).
77. H. Tanigawa, K. Shiba, A. Мцslang, R. Stoller, R. Lindau, M. Sokolov, G. Odette, R. Kurtz, and S. Jitsukawa, Status and key issues of reduced activation ferritic/martensitic steels as the structural material for a DEMO blanket, *J. Nuclear Mater.*, **417**: 9 (2011);
https://doi.org/10.1016/j.jnucmat.2011.05.023

78. M. Leont'eva-Smirnova, A. Ioltukhovskiy, G. A. Arutiunova, A. Tselischev, and V. Chernov, Investigation of heat treatment conditions on the structure of 12% chromium reduced activation steels, *J. Nuclear Mater.*, **307**: 466 (2002); https://doi.org/10.1016/s0022-3115(02)01139-x
79. W. Yan, W. Wang, Y. Shan, and K. Yang, Microstructural stability of 9–12% Cr ferrite/martensite heat-resistant steels, *Front. Mater. Sci.*, **1**: 1 (2013); https://doi.org/10.1007/s11706-013-0189-5
80. C. Kocer, T. Abe, and A. Soon, The Z-phase in 9–12% Cr ferritic steels: A phase stability analysis, *Mater. Sci. Eng. A*, **505**: 1 (2009); https://doi.org/10.1016/j.msea.2008.10.028
81. E. Evangelista, H. Mcqueen, M. Niewczas, and M. Cabibbo, Hot Workability of 2304 and 2205 duplex stainless steels, *Canadian Metallurgical Quarterly*, **43**: 339 (2004); https://doi.org/10.1179/cmq.2004.43.3.339
82. Y. Son, Y.K. Lee, K.-T. Park, C.S. Lee, and D. Shin, Ultrafine grained ferrite–martensite dual phase steels fabricated via equal channel angular pressing: Microstructure and tensile properties, *Acta Mater.*, **53**: 3125 (2005); https://doi.org/10.1016/j.actamat.2005.02.015
83. H. Zheng, X. Ye, J.-C. Li, L.-Z. Jiang, Z. Liu, W. Guanqi, and B. Wang, Effect of carbon content on microstructure and mechanical properties of hot-rolled low carbon 12Cr–Ni stainless steel, *Mater. Sci. Eng. A*, **527**: 7407 (2010); https://doi.org/10.1016/j.msea.2010.08.023
84. V.B. Molodkin, H.I. Nizkova, Ye.I. Bogdanov, S.I. Olikhovskii, S.V. Dmitriev, M.G. Tolmachev, V.V. Lizunov, Ya.V. Vasylyk, A.G. Karpov, and O.G. Voytok, The physical nature and new capabilities of use of effects of asymmetry of azimuthal dependence of total integrated intensity of dynamical diffraction for diagnostics of crystals with the disturbed surface layer and defects, *Usp. Fiz. Met.*, **18**, No. 2: 177 (2017); https://doi.org/10.15407/ufm.18.02.177
85. V.V. Lizunov, I.M. Zabolotnyy, Ya.V. Vasylyk, I.E. Golentus, and M.V. Ushakov, Integrated diffractometry: achieved progress and new performance capabilities, *Prog. Phys. Met.*, **20**, No. 1: 75 (2019); https://doi.org/10.15407/ufm.20.01.075
86. V.A. Tatarenko and C.L. Tsynman, Strain-induced and blocking effects in thermodynamics of the ordering and precipitation reactions within the off-stoichiometric close-packed-metal hydrides, *Solid State Ionics*, **101–103**, Pt. 2: 1061 (1997); https://doi.org/10.1016/s0167-2738(97)00376-7
87. T.M. Radchenko, O.S. Gatsenko, V.V. Lizunov, and V.A. Tatarenko, Martensitic α''-$Fe_{16}N_2$-type phase of non-stoichiometric composition: current status of research and microscopic statistical-thermodynamic model, *Prog. Phys. Met.*, **21**, No. 4: 580 (2020); https://doi.org/10.15407/ufm.21.04.580
88. K.H. Levchuk, T.M. Radchenko, and V.A. Tatarenko, High-temperature entropy effects in tetragonality of the ordering interstitial–substitutional solution based on body-centred tetragonal metal, *Metallofiz. Noveishie Tekhnol.*, **43**, No. 1: 1 (2021); https://doi.org/10.15407/mfint.43.01.0001
89. T.M. Radchenko, O.S. Gatsenko, V.V. Lizunov, and V.A. Tatarenko, Research trends and statistical-thermodynamic modeling the α''-$Fe_{16}N_2$-based phase for permanent magnets, *Fundamentals of Low Dimensional Magnets* (Eds. R.K. Gupta,

S.R. Mishra, and T.A. Nguyen) (Boca Raton, USA: CRC Press: 2022), Ch. 18, p. 343; https://doi.org/10.1201/9781003197492-18
90. A. Naizabekov, S. Lezhnev, E. Panin, and I. Volokitina, Structure and mechanical properties of steel in the process 'pressing–drawing', *J. Mater. Eng. Perform.*, **28**: 1762 (2019); https://doi.org/10.1007/s11665-019-3880-6
91. A. Volokitin, A. Naizabekov, and S. Lezhnev, Research of a new method of deformation pressing–drawing on mechanical properties of steel wire, *Proc. of the Metal 2013 — 22nd Int. Conf. on Metallurgy and Materials (15–17 May 2013)* (Brno: 2013); p. 376.
92. T. Hickel, B. Grabowski, F. Kormann, and J. Neugebauer, Advancing density functional theory to finite temperatures: methods and applications in steel design, *J. Phys.: Cond. Matter*, **24**: 053202 (2012); https://doi.org/10.1088/0953-8984/24/5/053202
93. J. Yoo and Kyung-Tae Park, Microband-induced plasticity in a high Mn–Al–C light steel, *Mater. Sci. Eng. A*, **496**: 417 (2008); https://doi.org/10.1016/j.msea.2008.05.042
94. J.D. Yoo, S.W. Hwang, and K.T. Park, Origin of extended tensile ductility of a Fe–28Mn–10Al–1C steel, *Met. Mater. Trans. A*, **40**: 1520 (2009); https://doi.org/10.1007/s11661-009-9862-9
95. S. Nambu, N. Shibuta, M. Ojima, J. Inoue, T. Koseki, and H. Bhadeshia, In situ observations and crystallographic analysis of martensitic transformation in steel, *Acta Mater.*, **61**: 4831 (2013); https://doi.org/10.1016/j.actamat.2013.04.065
96. *Martensitic Transformation* (Eds. M.E. Fine, M. Meshii, and C.M. Wayman) (New York: Academic Press: 1978); https://doi.org/10.1016/b978-0-12-519850-9.X5001-7
97. A.P. Gulyaev and N.A. Kozlova, *Spetsial'nyye Stali i Splavy* [Special Steels and Alloys] (Metallurgy: 1966) (in Russian).
98. M.A. Filippov, V.S. Litvinov, and Yu.R. Nemirovsky, *Stalis Metastabil'nym Austenitom* [Steels with Metastable Austenite] (Metallurgy: 1988) (in Russian).
99. A.P. Gulyaev and I.Ya. Georgieva, O Vzaimosvyazi mezhdu Kinetikoy i Strukturoy pri Martensitnykh Prevrashcheniyakh [On the Relationship between the Kinetics and Structure at the Martensitic Transformations], *Phys. Met. Mater. Sci.* (1971) (in Russian).
100. V.V. Sagaradze and A.I. Uvarov, *Uprochnenie Austenitnykh Staley* [Strengthening of Austenitic Steels] (Nauka: 1989) (in Russian).
101. V.F. Terentiev, *Ustalostnaya Prochnost' Metallov i Splavov* [Fatigue Strength of Metals and Alloys] (Intermet, Engineering: 2002) (in Russian).
102. E. Scheil, Ьber die umwandlung des austenits in martensit in eisen-nickellegierungen unter belastung, *Zeitschrift fьr Anorganische und Allgemeine Chemie (ZAAC)*, **207**, No. 1: 21 (1932) (in German); https://doi.org/10.1002/zaac.19322070103
103. B.R. Banerjee, J.M. Capenos, and J.J. Hauser: *Application of Fracture Toughness Parameters to Structural Metals* (Gordon and Breach: 1966), p. 373.
104. J. Tamura, T. Maki, and H. Hato, K. Aburai, *J. Jpn. Inst. Met. Mater.*, **33**: 1383 (1969).
105. B. Rao and M. Rashid, Direct observations of deformation-induced retained austenite transformation in a vanadium-containing dual-phase steel, *Mater. Characterization*, **39**: 435 (1997); https://doi.org/10.1016/S1044-5803(97)00156-3

106. V.F. Terentiev, *Prochnost' Splavov* [Strength of Alloys] (MISiS: 1997) (in Russian).
107. L.I. Lysak and B.I. Nikolin, Izuchenie Rel'efa pri γ→ε Prevrashchenii na Monokristallakh Stali Fe–Mn–C [Study of a Relief during the γ→ε Transformation on the Fe–Mn–C Steel Single Crystals], *Phys. Met. Mater. Sci.* (1964) (in Russian).
108. V.Yu. Danilchenko, V.F. Mazanko, O.V. Filatov, and V.E. Iakovlev, Effect of cyclic martensitic γ–ε transformations on diffusion characteristics of cobalt in an iron–manganese alloy, *Prog. Phys. Met.*, **20**, No. 3: 426 (2019); https://doi.org/10.15407/ufm.20.03.426
109. V.Y. Bondar, V.E. Danilchenko, V.F. Mazanko, O.V. Filatov, and V.E. Iakovlev, Effect of cyclic martensitic γ–ε–γ transformations on diffusion characteristics of carbon in an iron–manganese alloy, *Prog. Phys. Met.*, **19**, No. 1: 70 (2018); https://doi.org/10.15407/ufm.19.01.070
110. T. Suzuki, H. Kojima, K. Suzuki, T. Hashimoto, and M. Ichihara, An experimental study of the martensite nucleation and growth in 18/8 stainless steel, *Acta Met.*, **25**: 1151 (1977); https://doi.org/10.1016/0001-6160(77)90202-4
111. K.P. Staudhammer, L.E. Murr, and S.S. Hecker, Nucleation and evolution of strain-induced martensitic (b.c.c.) embryos and substructure in stainless steel: A transmission electron microscope study, *Acta Met.*, **31**: 267 (1983); https://doi.org/10.1016/0001-6160(83)90103-7
112. H. Biermann, J. Solarek, and A. Weidner, SEM investigation of high-alloyed austenitic stainless cast steels with varying austenite stability at room temperature and 100 °C, *Steel Research Int.*, **83**: 512 (2021); https://doi.org/10.1002/srin.201100293
113. I. Volokitina, A. Kolesnikov, R. Fediuk, S. Klyuev, L. Sabitov, A. Volokitin, T. Zhuniskaliyev, B. Kelamanov, D. Yessengaliev, A. Yerzhanov, and O. Kolesnikova, Study of the properties of antifriction rings under severe plastic deformation, *Materials*, **15**: 2584 (2022); https://doi.org/10.3390/ma15072584
114. M. Furukawa, Z. Horita, M. Nemoto, and T.G. Langdon, The use of severe plastic deformation for microstructural control, *Mater. Sci. Eng. A*, **324**: 82 (2002); https://doi.org/10.1016/S0921-5093(01)01288-6
115. A.P. Zhilyaev and T.G. Langdon, Using high-pressure torsion for metal processing: Fundamentals and applications, *Prog. Mater. Sci.*, **53**: 893 (2008); https://doi.org/10.1016/j.pmatsci.2008.03.002
116. A. Alhamidi and Z. Horita, Grain refinement and high strain rate superplasticity in alumunium 2024 alloy processed by high-pressure torsion, *Mater. Sci. Eng. A*, **622**: 139 (2015); https://doi.org/10.1016/j.msea.2014.11.009
117. Yu.S. Projdak, V.Z. Kutsova, T.V. Kotova, H.P. Stetsenko, and V.V. Prutchykova, Regularities of formation of structure, texture and properties under the combined plastic deformation of the low-carbon and ultralow-carbon steels for cold press forming, *Prog. Phys. Met.*, **20**: 213 (2019); https://doi.org/10.15407/ufm.20.02.213
118. A. Naizabekov, A. Arbuz, S. Lezhnev, E. Panin, and I.Volokitina, The development and testing of a new method of qualitative analysis of the microstructure quality, for example of steel AISI 321 subjected to radial shear rolling, *Phys. Scr.*, **94**: 105702 (2019); https://doi.org/10.1088/1402-4896/ab1e6e

119. A. Volokitin A. Naizabekov I. Volokitina, S. Lezhnev, and E. Panin, Thermomechanical treatment of steel using severe plastic deformation and cryogenic cooling, *Mater. Lett.*, **304**: 130598 (2021); https://doi.org/10.1016/j.matlet.2021.130598
120. C. Keller K. Tabalaiev, Gaյl Marnier, J. Noudem, X. Sauvage, and E. Hug, Influence of spark plasma sintering conditions on the sintering and functional properties of an ultra-fine grained 316L stainless steel obtained from ball-milled powder, *Mater. Sci. Eng. A*, **665**: 125 (2016); https://doi.org/10.1016/j.msea.2016.04.039
121. H. Ni, H. He, G. Li, and J. Liu, Preparation of nanocrystalline 430L stainless steel by HEBM and SPS, *J. Iron Steel Res. Int.*, **15**: 73 (2008); https://doi.org/10.1016/s1006-706x(08)60147-8
122. R.Z. Valiev, R.K. Islamgaliev, and I.V. Alexandrov, Bulk nanostructured materials from severe plastic deformation, *Prog. Mater. Sci.*, **45**: 103 (2000); https://doi.org/10.1016/s0079-6425(99)00007-9
123. Y. Estrin and A. Vinogradov, Fatigue behaviour of light alloys with ultrafine grain structure produced by severe plastic deformation: an overview, *Int. J. Fatigue*, **32**: 898 (2010); https://doi.org/10.1016/j.ijfatigue.2009.06.022
124. I. Volokitina, A. Volokitin, A. Naizabekov, and E.Panin, *J. Chem. Technol. Metallurgy*, **56**: 410 (2021).
125. *Ultrafine Grained Materials III* (Eds. Y.T. Zhu, T.G. Langdon, R.Z. Valiev, S.L. Semiatin, D.H. Shin, T.C. Lowe) (Charlotte, North Carolina: TMS: 2004).
126. A.B. Nayzabekov and I.E. Volokitina, Effect of the initial structural state of Cr–Mo high-temperature steel on mechanical properties after equal-channel angular pressing, *Phys. Metals Metallogr.*, **120**: 177 (2019); https://doi.org/10.1134/s0031918x19020133
127. Y. Estrin and A. Vinogradov, Extreme grain refinement by severe plastic deformation: a wealth of challenging science, *Acta Mater.*, **61**: 782 (2013); https://doi.org/10.1016/j.actamat.2012.10.038
128. Y. Beygelzimer, V. Varyukhin, S. Synkov, and D. Orlow, Useful properties of twist extrusion, *Mater. Sci. Eng. A*, **503**: 14 (2009); https://doi.org/10.1016/j.msea.2007.12.055
129. L. Kecskes, Kyu C. Cho, R. Dowding, B. Schuster, R. Valiev, and Q. Wei, Grain size engineering of bcc refractory metals: top-down and bottom-up — application to tungsten, *Mater. Sci. Eng. A*, **467**: 33 (2007); https://doi.org/10.1016/j.msea.2007.02.099
130. T.G. Langdon, The principles of grain refinement in equal-channel angular pressing, *Mater. Sci. Eng. A*, **462**: 3 (2007); https://doi.org/10.1016/j.msea.2006.02.473
131. Z. Fan, T. Hao, S. X. Zhao, G. Luo, C. S. Liu, and F. Qianfeng, The microstructure and mechanical properties of T91 steel processed by ECAP at room temperature, *J. Nuclear Mater.*, **434**: 417 (2013); https://doi.org/10.1016/j.jnucmat.2012.12.009
132. K. Edalati, A. Bachmaier, V.A. Beloshenko, Y. Beygelzimer, V.D. Blank, W.J. Botta, K. Bryła, J. Čнžek, S. Divinski, N.A. Enikeev, Y. Estrin, G. Faraji, R.B. Figueiredo, M. Fuji, T. Furuta, T. Grosdidier, J. Gubicza, A. Hohenwarter, Z. Horita, J. Huot, Y. Ikoma, M. Janeček, M. Kawasaki, P. Král, S. Kuramoto, T.G. Langdon, D.R. Leiva, V.I. Levitas, A. Mazilkin, M. Mito, H. Miyamoto, T. Nishizaki, R. Pippan, V.V. Popov, E.N. Popova, G. Purcek, O. Renk, Б. Révész, X. Sauvage, V. Sklenicka, W. Skrotzki, B.B. Straumal, S. Suwas, L.S. Toth, N. Tsuji,

R.Z. Valiev, G. Wilde, M.J. Zehetbauer, and X. Zhu, Nanomaterials by severe plastic deformation: review of historical developments and recent advances, *Mater. Res. Let.*, **10**, No. 4: 163 (2022); https://doi.org/10.1080/21663831.2022.2029779

133. G.G. Mayer, E.G. Astafurova, and E.V. Naidenkin, *Termicheskaya Stabil'nost' Submikrokristallicheskoy Struktury, Sformirovannoy Metodom Ravnokanal'nogo Uglovogo Pressovaniya v Nizkouglerodistykh Stalyakh s Razlichnym Fazovym Sostavom* [Thermal Stability of Submicrocrystalline Structure Formed by Equal-Channel Angular Pressing in Low Carbon Steels with Different Phase Composition] (Metal Processing: 2013) (in Russian).
134. G. Yang, C. Huang, C. Wang, L. Y. Zhang, C. Hu, Z. Zhang, and S. Wu, *Mater. Sci. Eng. A*, **515**: 199, (2011); https://doi.org/10.1016/j.msea.2009.03.031
135. E.G. Astafurova, G.G. Zakharova, E.V. Naydenkin, G.I. Raab, P.D. Odessky, and S.V. Dobatkin, Structural peculiarities and mechanical behavior of Fe–Mo–V–Nb–C steel after equal channel angular pressing, *Lett. Mater.*, **1**, No. 4: 198 (2011); https://doi.org/10.22226/2410-3535-2011-4-198-202
136. J. Li, M. Umemoto, Y. Todaka, K. Fujisaku, and K. Tsuchiya, *Mater. Sci.*, **18**: 577, (2008).
137. L.A. Maltseva and K.D. Khramtsova, *Formirovanie Submikrokristallicheskogo Sostoyaniya v Austenitnoy Metastabil'noy Stali Metodami Intensivnoy Plasticheskoy Deformatsii* [Formation of Submicrocrystalline State in Austenitic Metastable Steel by Severe Plastic Deformation Methods] (Vector of Science, Togliatti State University: 2013) (in Russian).
138. M. Eskandari, A. Kermanpur, and A. Najafizadeh, Formation of nano-grained structure in a 301 stainless steel using a repetitive thermo-mechanical treatment, *Mater. Lett.*, **63**: 1442 (2009); https://doi.org/10.1016/j.matlet.2009.03.043
139. B. Kumar, S. Das, S. Sharma, and J.K. Sahu, Effect of thermal cycles on heavily cold deformed AISI 304L austenitic stainless steel, *Mater. Sci. Eng. A*, **527**: 875 (2010); https://doi.org/10.1016/j.msea.2009.08.075
140. M. Gao, C. N. Reid, M. Jahedi, and Y. Li, Estimating equilibration times and heating/cooling rates in heat treatment of workpieces with arbitrary geometry, *J. Mater. Eng. Perform.*, **9**: 62 (2000); https://doi.org/10.1361/105994900770346295
141. S. Dobatkin, O.V. Rybal'chenko, N. Enikeev, A.A. Tokar', and M. Abramova, Formation of fully austenitic ultrafine-grained high strength state in metastable Cr–Ni–Ti stainless steel by severe plastic deformation, *Mater. Lett.*, **166**: 276, (2016); https://doi.org/10.1016/j.matlet.2015.12.094
142. S.-J. Lee, Y.-M. Park, and Y.-K. Lee, Reverse transformation mechanism of martensite to austenite in a metastable austenitic alloy, *Materials Science and Engineering A*, **515**: 32, (2009); https://doi.org/10.1016/j.msea.2009.02.010

Received 12.08.2022;
in final version, 13.10.2022

І.Є. Волокітіна[1], *А.В. Волокітін*[2], *Є.А. Панін*[2]
[1]Рудненський індустріальний інститут,
вул. 50 років Жовтня, 38; 111500 Рудний, Казахстан
[2]Карагандинський індустріальний університет,
просп. Республіки, 30; 101400 Темиртау, Казахстан

МАРТЕНСИТНІ ПЕРЕТВОРЕННЯ У НЕІРЖАВІЙНИХ КРИЦЯХ

Наразі інтенсивно розвивається напрям досліджень матеріалів, у яких спостерігаються мартенситні перетворення. Це пов'язано з тим, що в процесі мартенситних перетворень у багатьох матеріалах утворюються різні дефекти кристалічної будови (двійники, дислокації, дефекти пакування тощо), які разом із фраґментацією зерен приводять до істотного підвищення міцнісних властивостей. Широка поширеність мартенситних перетворень привела до дослідження особливостей дефектної мікроструктури та змін механічних властивостей матеріалів у процесі мартенситних перетворень. Це сприяло тому, що теорія мартенситних перетворень зайняла ключове місце в науці про структуру та властивості кристалічних тіл. Діапазон робочих температур криць такого класу обмежений знизу їхньою схильністю до низькотемпературного окрихчування (холодноламкости) за радіаційних впливів, а зверху — рівнем тривалої міцности (жаротривкости). У зв'язку з цим на сьогоднішній день підвищену увагу фахівців у галузі фізики конденсованого стану до феритно-мартенситних криць викликано необхідністю виявлення механізмів формування стійких за робочих температур мікроструктури та функціональних властивостей криць, а також пошуку резервів підвищення їхньої жаротривкости зі збереженням достатнього рівня пластичности.

Ключові слова: неіржавійна криця, мартенсит, мартенситне перетворення, мікроструктура, відпал, жаротривкість.